Voltage-dependent conformational changes of Kv1.3 channels activate cell proliferation

Journal:	*Journal of Cellular Physiology*
Manuscript ID	Draft
Wiley - Manuscript type:	Original Research Article
Date Submitted by the Author:	n/a
Complete List of Authors:	Cidad, Pilar; Universidad de Valladolid, Departamento de Bioquímica y Biología Molecular y Fisiología ; CSIC, Instituto de Biología y Genética Molecular, IBGM Alonso, Esperanza; Universidad de Valladolid, Departamento de Bioquímica y Biología Molecular y Fisiología ; CSIC, Instituto de Biología y Genética Molecular Arévalo-Martínez, Marycarmen; Universidad de Valladolid, Departamento de Bioquímica y Biología Molecular y Fisiología ; CSIC, Instituto de Biología y Genética Molecular, IBGM Calvo, Enrique; Fundacion Centro Nacional de Investigaciones Cardiovasculares Carlos III, Unidad de Proteómica de la Fuente, Miguel; Universidad de Valladolid, Departamento de Biología Celular ; CSIC, Instituto de Biología y Genética Molecular, IBGM Perez-Garcia, M. Teresa; Universidad de Valladolid, Departamento de Bioquímica y Biología Molecular y Fisiología ; CSIC, Instituto de Biología y Genética Molecular, IBGM López-López, José; Universidad de Valladolid, Departamento de Bioquímica y Biología Molecular y Fisiología ; CSIC, Instituto de Biología y Genética Molecular; IBGM
Key Words:	Kv channels, cell proliferation, membrane potential, IQGAP3

Voltage-dependent conformational changes of Kv1.3 channels activate cell proliferation

Running title: Kv1.3 channels as voltage sensors for proliferation

Pilar Cidad[1,3], Esperanza Alonso[1,3], Marycarmen Arévalo-Martínez[1,3], Enrique Calvo[4], Miguel Ángel de la Fuente[2,3], María Teresa Pérez-García[1,3,*] and José Ramón López-López[1,3,*].

Departamento de Bioquímica y Biología Molecular y Fisiología (1) and Biología Celular (2), and Instituto de Biología y Genética Molecular (3), Universidad de Valladolid and CSIC, Valladolid, and (4) Unidad de Proteómica, Centro Nacional de Investigaciones Cardiovasculares, CNIC, Madrid, SPAIN

*equal senior authors

Correspondence:
Dr M. Teresa Pérez-García
Departamento de Bioquímica y Biología Molecular y Fisiología
Universidad de Valladolid
Edificio IBGM, c/ Sanz y Forés, 3
47003 Valladolid, SPAIN
tperez@ibgm.uva.es. ORCID ID: 0000-0001-8540-8117

ACKNOWLEDGEMENTS

We thank Dr CG Nichols for kindly provide the K_{ATP} plasmids and Dr. Miguel Holmgren for helpful discussions on the manuscript. We also thank Pablo Fernández and Javier Martínez for their help with some of the experiments. Supported by grants BFU2016-75360-R (MINECO) and VA114P17 (Junta de Castilla y León). The CNIC is supported by the Ministry of Economy, Industry and Competitiveness (MEIC) and the Pro-CNIC Foundation and is a Severo Ochoa Center of Excellence (MINECO award SEV-2015-0505).

CONFLICT OF INTEREST

The authors declare no competing financial interests.

DATA AVAILABILITY STATEMENT

The data that support the findings of this study are available from the corresponding author upon reasonable request.

AUTHOR CONTRIBUTIONS (CRedIT roles)

Conceptualization, PC, MAF, MTP-G and JRL-L. ; Methodology: PC, MTP-G and JRL-L.; Formal Analysis: PC and MTP-G; Investigation: PC, EA, MA-M, MAF, MTP-G and JRL-L; Software: JRL-L; Writing – Review & Editing: PC, MTP-G and JRL-L; Visualization: PC, MTP-G and JRL-L; Supervision: PC, MAF, MTP-G and JRL-L; Funding Acquisition: MTP-G and JRL-L.

ABSTRACT

The voltage-dependent potassium channel Kv1.3 has been implicated in proliferation in many cell types, based on the observation that Kv1.3 blockers inhibited proliferation. By modulating membrane potential, cell volume and/or Ca^{2+} influx, K^+ channels can influence cell cycle progression. Also, non-canonical channel functions could contribute to modulate cell proliferation independently of K^+ efflux. The specificity of the requirement of Kv1.3 channels for proliferation suggests the involvement of molecule-specific interactions, but the underlying mechanisms are poorly identified. Heterologous expression of Kv1.3 channels in HEK cells has been shown to increase proliferation independently of K^+ fluxes. Likewise, some of the molecular determinants of Kv1.3-induced proliferation have been located at the C-terminus region, where individual point mutations of putative phosphorylation sites (Y447A and S459A) abolished Kv1.3-induced proliferation.

Here we investigated the mechanisms linking Kv1.3 channels to proliferation looking over the correlation between Kv1.3 voltage-dependent molecular dynamics and cell cycle progression. Using transfected HEK cells, we analyzed both the effect of changes in resting membrane potential on Kv1.3-induced proliferation and the effect of mutated Kv1.3 channels with altered voltage dependence of gating. We conclude that voltage-dependent transitions of Kv1.3 channels enable the activation of proliferative pathways. We also found that Kv1.3 associates with IQGAP3, a scaffold protein involved in proliferation, and that membrane depolarization facilitates their interaction. The functional contribution of Kv1.3-IQGAP3 interplay to cell proliferation was demonstrated both in HEK cells and in vascular smooth muscle cells. Our data indicate that voltage-dependent conformational changes of Kv1.3 are an essential element in Kv1.3-induced proliferation.

INTRODUCTION

The voltage-dependent potassium channels (Kv channels) comprise a large family of channels, which are expressed in both excitable and non-excitable cells. In excitable cells, they regulate action potentials frequency and duration by means of their contribution to resting membrane potential (E_M) control. This same ability of sensing and modulating E_M allows Kv channels to contribute to processes ranging from secretion to cell migration and proliferation in non-excitable tissues (Urrego, Tomczak, Zahed, Stühmer, & Pardo, 2014; Wulff, Castle, & Pardo, 2009), although in a different time scale. Rapid changes in E_M (in the millisecond range) are best known in excitable cells and E_M cyclic fluctuations on a much longer timescale can be observed in all cells as a consequence of cyclic changes in the expression and/or activity of ion channels and transporters.

The association between E_M and cell cycle progression was first suggested in the late 60's in the pioneer studies of Cone (Cone, Jr., 1970). He postulated that the observed variations of E_M along the cell cycle were directly related to progression through G1/S and G2/M transitions. Moreover, he demonstrated that membrane hyperpolarization reversibly blocked DNA synthesis and mitosis, while membrane depolarization could induce mitosis in mature neurons (Cone & Cone, 1976). In general, terminally differentiated, quiescent cells tend to show a strongly hyperpolarizing E_M, whereas embryonic, stem, and tumour cells tend to be depolarized (Levin, 2014), but the picture is complicated because the relationships between the cell cycle–dependent changes in E_M and cell proliferation are still poorly understood (Levin, 2014; McCaig, Song, & Rajnicek, 2009; Urrego, Sánchez, Tomczak, & Pardo, 2017). Importantly, E_M is not simply a readout but also a functional determinant of the cell cycle progression, because of several mechanisms coupling voltage potential changes to downstream signalling cascades. The identification of the ion channel genes that determine E_M states along cell cycle, the transduction mechanisms that sense E_M changes and the downstream targets will contribute to integrate our knowledge of the electrical and

chemical signals leading to proliferation. In this regard, the molecular, physiological and pharmacological characterization of the ion channels contributing to E_M modulation has been disclosed in many preparations, as well as some of the downstream signalling pathways (reviewed in Blackiston et al., 2009**;** Levin, 2014)**.** However, while our knowledge regarding the biochemical checkpoint machinery has increased substantially, the role of bioelectrical signals and the complex bidirectional relationship between ion channels function and cell cycle progression is ill defined (McCaig et al., 2009; Sundelacruz, Levin, & Kaplan, 2009).

K^+ fluxes through Kv channels are important for setting E_M and the driving force for Ca^{2+} influx, as well as for volume regulation of growing cells, and all these mechanisms contribute in many different ways to cell cycle progression (Lang et al., 2007; Ouadid-Ahidouch & Ahidouch, 2013). In addition, emerging evidence suggests that K^+ channels can control cell proliferation through other signaling mechanisms independent of ion fluxes (Hegle, Marble, & Wilson, 2006; Kaczmarek, 2006; Millership et al., 2011; Urrego et al., 2014). Their large variety and their functional flexibility together with their plasma membrane location, makes them suitable for coordinating multiple signaling pathways, integrating intra and extracellular signals.

Among Kv channels, Kv1.3 was the first channel reported to modulate cell proliferation (DeCoursey, Chandy, Gupta, & Cahalan, 1984). Kv1.3 channels have a relatively limited distribution pattern (https://gtexportal.org/home/gene/KCNA3). They are mainly found in various cell types in the immune system cells, in most cases as the only Kv channel expressed (Cahalan & Chandy, 2009; Feske, Wulff, & Skolnik, 2015). Besides, Kv1.3 channels are expressed at low levels in nervous system, lung and smooth muscle, contributing to heterotetrameric Kv1 channels. Their relevant contribution to immune system function has boosted the development of selective Kv1.3 blockers as immunomodulatory agents. All these inhibitors block K^+ permeation by direct channel pore occlusion. In addition, their blocking effects can also involve state-dependent mechanisms, such as the inhibition of the closed deactivated state in the case of the

antimycobacterial clofazimine (Faouzi, Starkus, & Penner, 2015), or the preferential binding to the inactivated state of the phenoxyalkoxypsoralens such as Psora-4 and PAP-1 (Schmitz et al., 2005).

After their initial description (DeCoursey et al., 1984), Kv1.3 channels have been described as modulators of cell proliferation in many different tissues, including several cancer cell types, vascular smooth muscle cells (VSMCs), microglia, oligodendrocyte progenitors and macrophages (reviewed in Pérez-García et al., 2018). Of interest, this pro-proliferative effect of Kv1.3 can be reproduced upon heterologous expression of the channel in HEK293 cells, providing a convenient tool to explore the molecular determinants of Kv1.3-induced proliferation. Kv1.3-induced proliferation of HEK293 cells does not require K^+ fluxes, but needs an intact voltage-sensing mechanism (Cidad et al., 2012). In fact, Kv1.3 blockers inhibit Kv1.3-induced proliferation because they also affect voltage-dependent gating of Kv1.3 channels (Cidad et al., 2012). The molecular determinants of Kv1.3-induced proliferation have been located at the cytosolic-C-terminal domain, where two individual point mutations of putative phosphorylation sites (Y447A and S459A) abolished Kv1.3-induced proliferation (Jiménez-Pérez et al., 2016). We postulated that Kv1.3-induced proliferation involves the accessibility of key docking sites at the C-terminus (the signaling domain), which could be regulated by voltage-dependent conformational changes. When the change takes place, these Kv1.3 residues can undergo MEK/ERK dependent phosphorylation, which initiates a signaling pathway leading to proliferation (Jiménez-Pérez et al., 2016). While the available data can fit this theory, there are several assumptions that have not been experimentally demonstrated. First, the hypothesis presumes that the role of Kv1.3 channels in proliferation is dependent on its capability of sensing voltage changes, because gating deficient Kv1.3 channels cannot induce proliferation. In this context, Kv1.3 channels would behave as molecular switches modulating signaling pathways relevant for promoting proliferation, and the transition between the ON and OFF states of the channel should be voltage dependent. Also, the activation of the

Kv1.3 molecular switch would require the participation of some still unidentified Kv1.3 associated proteins that would activate signaling pathways linked to proliferation such as MEK/ERK.

Here, we pursue to answer these questions going deeper into the mechanisms involved in Kv1.3 proliferation. First, we directly tested the hypothesis that Kv1.3 voltage sensing is required for activating cell proliferation, by analyzing 1) the effect of changes on E_M on Kv1.3-induced proliferation, and 2) the effect of changing Kv1.3 voltage sensitivity (by introducing several mutations in the protein) on the activation of proliferation. Second, looking for potential Kv1.3 channel partners, we found a significant interaction with IQGAP3, a scaffold protein whose expression seems to be specifically confined to proliferating cells (Nojima et al., 2008). IQGAP3 expression has been associated with proliferation both in normal and cancer cells, showing a positive correlation with the proliferative capacity of the cells, while its knockdown in cancer cells significantly inhibited proliferation and migration (Xu et al., 2016). Moreover, It has been described that IQGAP3 regulates the promotion of cell proliferation through Ras-dependent ERK activation (Fang, Zhang, Thisse, Bloom, & Thisse, 2015; Hedman, Smith, & Sacks, 2015; Nojima et al., 2008; Smith, Hedman, & Sacks, 2015). We have explored the possible implication of IQGAP3 to Kv1.3-induced proliferation. Our findings confirm the existence of an association between these two proteins that is facilitated by membrane depolarization. Moreover, functional studies confirm IQGAP3 contribution to Kv1.3-induced proliferation not only in HEK cells but also in vascular smooth muscle cells (VSMCs). These later results support the possible extrapolation of the mechanisms linking Kv1.3 activation and cell proliferation proposed in heterologous expression systems to native cells.

MATERIALS AND METHODS

Plasmid construction and mutant design

pcDNA3.1-Kir6.2WT, pcDNA3.1-Kir6.2G334D and pECE-SUR1 vectors were kindly provided by Dr. Colin Nichols (St. Louis, MO). For creating Kv1.3 gating-mutant channels, three single mutations of residues located in S3 or S4 showing a rightward shift of the activation curve were selected from previous work (Li-Smerin, Hackos, & Swartz, 2000), and the corresponding mutations (D285A (DA), A288Y (AY) and R332A (RA)) were generated in the Kv1.3 channel (See scheme in Figure 3A). We used either the pEGFP-N3-mKv1.3 (wild type channel) or the pEGFP-N3-mKv1.3WF (a non-conducting, pore-mutant channel) vectors as templates (Cidad et al., 2012). Phusion Site-Directed Mutagenesis Kit (Thermo Scientific) was used to generate the required mutants by PCR of the vector templates, with the following primers:

D285A: FW 5'-GAACTTGATAG***c***CATTGTGGCCATCATTCCTT-3´ and RE 5´-ATGATATTTCTG GAG AAG GTG GC-3´.

A288Y: FW 5'-TAGACATTGTG***ta***CATCATTCCTTATTTTATCACTC-3´and RE 5´-TCAAGTTCATGATATTTCTGGAG-3´.

R332A: FW 5'- GCT CTCC***gc***CCATTCTAAGGGGCTGC-3´ and RE 5´- TTGAAGATGC GGAAAACCCTTAC-3´.

For creating the gating-insensitive Kv1.3 mutants, the triple (R320N/L321A/R326I) S4 mutation previously described (Miller and Aldrich, 1996) was also introduced at the equivalent positions in the Kv1.3 channel (Figure 3A) by site-directed mutagenesis carried out with the QuikChange method (Stratagene, La Jolla, CA, USA). The pEGFP-N3-mKv1.3 vector was used as template (Cidad et al., 2012). For IQGAP3 expressing vectors, an EcoRI–XhoII fragment containing human IQGAP3 full length sequence was obtained by PCR using cDNA from HEK cell line and cloned into pDNA3-myc vector. An insert containing myc-IQGAP was digested from the previous vector with HindIII and XhoI restriction enzymes and then subcloned into the vector pEGFP-C1 (Clontech) to generate the pEGFP-myc-IQGAP3 final construct. All constructs were verified by

DNA sequencing. The pEFGP-N3 vector (Clontech) was used in control conditions. For some experiments, a construct expressing Kv1.3 as a fusion protein with Cherry and its control (pCherry-N1-hKv1.3 and pCherry-N1 respectively, Jiménez-Pérez et al., 2016) were also used.

HEK cell culture and transfection

HEK293T cells were obtained from ATCC® CRL-3216™and routinely checked for mycoplasma contamination with Venor®GeM Classic Mycoplasma Detection Kit (Minerva Biolabs, Ref: 11-1025). Cells were maintained in DMEM medium supplemented with 5% FBS, penicillin-streptomycin (100 units/ml each), 5 µg/ml Fungizone, and 2 mM L-glutamine at 37 °C in a 5% CO_2 humidified atmosphere. HEK cells were plated in 35 mm petri dishes until reaching a 70-80% confluency. The cells were then transiently transfected using Lipofectamine™ 2000 (Thermo Scientific) in a ratio 1:4 (µg DNA: µl Lipofectamine) following maunfacturer´s instructions. The transfection mixture was left for up to 24 h, and efficiency was quantified in each experiment by the detection of the GFP or Cherry fluorescence and was routinely found to be between 65%-85%. For the experiments coexpressing Kv1.3 or Kv1.3WF and KATP channels we used 1 µg of Kv1.3 alone or with 0.6 µg of SUR1 and 0.3 µg of Kir6.2 expressing vectors, and 1 µg of GFP vector was used, as control. In the experiments with the gating mutants 1 µg of DNA of each construct was used. For the IQGAP3 overexpression we put 1.8 µg of IQGAP3 plasmid alone or in combination with 0.3 µg of Kv1.3. In all the transfections, the amount of DNA in all plates and in all conditions was kept constant by adding an empty vector or a GFP vector.

VSMC obtention and culture

The detailed protocol for obtaining primary cultured VSMC from human vessels has been described elsewhere (Cidad et al., 2015; Miguel-Velado et al., 2005). Briefly, human arterial or vein samples belonging to the COLMAH collection (https://www.redheracles.net/plataformas/en_coleccion-muestras-arteriales-

humanas.html) were obtained from donors undergoing vascular surgery. Small pieces of these vessels free of endothelial and adventitial layers arteries were placed in a 35 mm culture dish covered with 2 % gelatin (Type B, bovine skin, Sigma) in DMEM supplemented with 20 % SFB, penicillin-streptomycin (100 U/ml), 5 µg/ml fungizone, and 2 mM L-glutamine at 37º C in a 5% CO2 humidified atmosphere. After 1-2 weeks, migration and proliferation of VSMC from the explants was apparent. When cells reached confluence, they were detached by trypsin-EDTA treatment (2-6 min) and seeded in a new culture plate at a 1/3 density in SMC-P-STIM medium (D-MEM medium supplemented with 5% FBS, penicillin-streptomycin (100U/ml each), 5 µg/ml fungizone, L-glutamine (2 mM), Insulin (5 µg/ml), bFGF (2ng/ml) and EGF (0.5 ng/ml). VSMC were subjected to several (4-8) passages without showing morphological changes.

siRNA experiments and Real Time PCR

Cells were transfected with 10 nM of siIQGAP3 and negative control siRNAs (sc-788744 and sc-37007 respectively, Santa Cruz Biotechnology) using Lifofectamine (Invitrogen) for HEK cells or TransIT-X2 (Mirus) for VSMCs. 48 h after transfection, cells were tripsinized as described above and plated on poly-l-lysine treated, 12 mm diameter coverslips for proliferation assays or used for mRNA expression to analyze siRNA efficiency.

Total RNA was isolated using TRIzol reagent (Invitrogen), reverse transcribed and mRNA levels were determined by qPCR with Taqman assays in a Rotor-Gene 3000 instrument (Corbett Research). Data were analyzed with the threshold cycle relative quantification method (ΔΔCt), normalized to an endogenous control (ribosomal protein L18), and expressed as $2^{-\Delta\Delta Ct}$ using the control, (untransfected cells) as calibrator. Taqman assays used were: IQGAP3 (Hs01553726_m1, Applied Biosystems) and RPL18 (Forward primer: 5'-aactgatgatgtgcgggttc-3', Reverse primer: 5'-cagctggtcgaaagtgagg-3' and Probe: 5'-ctgaaggtatgtgcactgcgcgtga-3')

Electrophysiological studies

Ionic currents were recorded at room temperature using the whole-cell or the perforated-patch configuration of the patch clamp technique as previously described (Cidad et al., 2012; Tajada et al., 2013). Briefly, transfected HEK cells plated on small poly-L-Lysine treated glass coverslips were placed at the bottom of a small recording chamber (0.2 ml) on the stage of an inverted microscope and perfused by gravity with the bath solution. Patch pipettes were made from borosilicate glass (2.0mmO.D, World Precision Instruments, Sarasota, FL, USA) and double pulled with the P-97 automatic puller (Sutter Instruments, Novato, CA, USA) to resistances ranging from 2 to 5 MΩ. Transfected cells were identified by GFP or Cherry fluorescence using a LED source. The composition of the bath solution was (in mM): 141 NaCl, 4.7 KCl, 1.2 $MgCl_2$, 1.8 $CaCl_2$, 10 glucose, and 10 HEPES, pH 7.4 with NaOH. For the whole-cell experiments the composition of the internal solution was (in mM): 125 KCl, 4 MgCl2, 10 HEPES, 10 EGTA, 5 MgATP, pH 7.2 with KOH. For the perforated-patch experiments, the pipette tip was briefly dipped in a solution containing (in mM): 40 KCl, 95 KGlutamate, 8 CaCl2, 10 HEPES, pH 7.2 with KOH, and backfilled with the same solution containing amphotericin B (480 µg/ml). Perforated-patch recordings were used for some voltage-clamp experiments and for all current-clamp experiments. Gating currents were recorded using N-methyl-D-glucamide (NMDG) solutions of the following composition (mM): 140 N-methyl-D-glucamide (NMDG), 1 MgCl2, 10 EGTA and 10 HEPES (pH 7.2 with ClH) for internal solution and 140 NMDG, 1 MgCl2, 1 CaCl2, 10 HEPES, 10 glucose (pH 7.4 with ClH) for bath solution.

Voltage-clamp experiments: Whole-cell currents were recorded using an Axopatch 200 patch clamp amplifier, filtered at 2 kHz (−3 db, 4-pole Bessel filter) and sampled at 10 kHz. When leak subtraction was performed, an online P/4 protocol was used. Recordings were digitized with a Digidata 1200 A/D interface driven by CLAMPEX 8 software (Axon Instruments). Holding potential was set at -80 mV. Outward K^+ currents were elicited by voltage-ramps of 1s duration from -60 to +80 mV applied every 20s. In

some cells full current/voltage curves were constructed from potentials ranging from −80 to +100mV in 10-mV steps of 500ms duration. For the characterization of the steady state inactivation, a two-pulse protocol was used, in which after 10s depolarizing pulses from -120 to +40 in 40 mV steps, a 200 ms depolarizing pulse to +40 was elicited, and the current amplitude of this pulse was expressed as a function of the voltage of the prepulse. Kv1.3 currents were defined by their sensitivity to the selective blockers 5-(4-phenoxybutoxy)psoralen (PAP-1; 100-200 nM) or Margatoxin (MgTx; 1-5 nM) .The effect of the blockers was tested in the full I/V curves and /or in voltage ramps, as well as in depolarizing pulses from a holding potential of −80 mV to +40 mV applied in 15s intervals.

Conductance curves were obtained from the I/V relationships or the voltage ramps. After normalization to the maximal conductance (G_{max}) data were fitted to a Boltzmann function to obtain the $V_{0.5}$ of activation and the slope of the curve. The conductance curves were averaged and fitted to a Boltzmann function to obtain the mean $V_{0.5}$ and slope values for each mutant channel. The values obtained in this way (with the fit of the averaged curves) were not different from those collected when the data obtained from the fit of each individual cell was used to calculate the average conductance curves in each condition (the average of the fitted curves, data not shown).

Gating currents from Kv1.3 and Kv1.3WF were recorded as previously described (Cidad et al., 2012). Patch pipettes had resistances ranging from 1 to 3 MΩ when filling with the internal solution. Capacity compensation was routinely used, and series resistance was between 2 and 8 MΩ for all recordings. For some experiments, currents were recording using 60-75% series resistance compensation. The voltage-dependence of Qon was studied 10 ms depolarizing pulses from a holding potential of -120, ranging from -80 to +40 mV in 20 mV intervals. Charge measures was obtained by integrating the on gating currents, and Charge-Voltage (Q/V) relationships were normalized to the maximum Q_{ON},. The voltage dependence of gating charge movement was obtained from the fit of the normalized Q/V curves to a Boltzmann function:

Current-clamp experiments: Resting membrane potential (E_M) was determined with perforated-patch experiments (to avoid dialysis of intracellular medium) in the current-clamp configuration as previously described (Cidad et al., 2010). Recordings were obtained with an Axopatch 700A patch-clamp amplifier. After obtaining a high-resistance seal, electrical access to cell cytoplasm was assessed by monitoring the increase in cell capacitance. At this point, the amplifier was switched to current-clamp mode (I=0) and membrane potential (E_m) was continuously recorded, in order to determine its resting value in control HEK cells or cells transfected with the different plasmids, as well as its changes in response to increased extracellular [K+] or application of selective Kv1.3 blockers at the indicated concentrations. For the high extracellular K^+ solutions, Na^+ concentration in the external solution was reduced equimolarly. The high Ca^{2+} content of the pipette solution (see above) ensures the correct performance of the perforate-patch technique, as accidental rupture of the patch (changing to whole-cell configuration) would lead to a sudden Ca^{2+} load and cell death.

Electrophysiological analyses were performed with both the CLAMPFIT subroutine of the PCLAMP software (Axon) and ORIGIN 7.5 software.

Proliferation studies

In the case of HEK cells, once transfected, cells were trypsinized, counted with a hemocytometer and seeded at a density of 50,000 cells/well on 12-mm poly-lysine-coated coverslips. Proliferation was determined 24 h after seeding cells using a commercial kit (ClickiT® EdU Imaging Cell Proliferation Assay, Invitrogen) following previously described protocols (Jiménez-Pérez et al., 2016). The percentage of cells at the S phase was quantified using 5-ethynyl-2′-deoxyuridine (EdU) incorporation for a 20-min period. Treatments with Kv1.3 blockers were applied during 24h and also in the 20 min period incubation with EdU. For the experiments with increased $[K^+]_e$, two different solutions, solution A (in mM: 114.9 NaCl, 0 KCl, 0.81 MgSO4 , 44 $NaHCO_3$,

0.91 NaH_2PO_4, 5.55 Glucose, 1 sodium pyruvate, 2.5x10-4 $Fe(NO_3)_3$ and 1.80 $CaCl_2$) and B (the same composition except for 0 NaCl and 114. 9 KCl) were mixed in order to get isosmotic solutions with the desired K^+ concentrations. This treatment was applied during the 20 min incubation with Edu.

In the case of human VSMCs, the percentage of cells at the S phase was quantified using EdU incorporation for longer periods of time (6-10h). 20,000-30,000 VSMCs (depending on cell size) were seeded onto poly-l-lysine coated coverslips (12 mm diameter) placed in wells with P-STIM media supplemented with 10% FBS. Next day, media was replaced with serum-free media, and proliferation was induced by addition of PDGF (20 ng/ml), alone or in combination with the Kv1.3 blocker PAP-1 (100nM) during 24 h, following by EdU incubation for at least another 6h.

After Edu incubation cells were fixed with 3.7 % formaldehyde and permeabilized with 0.5% Triton X-100. Incorporated Edu was detected fluorescence after incubation with a reaction buffer containing Alexa fluor reagent. Cells were incubated with Hoechst 33342 (1:3000) for 10 min at RT for counting nuclei and coverslips were mounted in Vectashiel (Vector Laboratories, INC., Burlingame, CA). Images were acquired with 10x (for HEK cells) or 4x (for VSMCs) objectives on a fluorescence microscope with Nis-element software (Nikon). Images were binarized to measure the % of stained area (for HEK cells) or the number of stained nuclei (for VSMCs) with a routine analysis created using the Fiji (Image J) software. Proliferation rate was estimated as the percentage of EdU positive cells (EdU+) from the total cell number stained with Hoechst. In each experiment, determinations were carried out in triplicates, and 4 to 5 images of each coverslips were acquired. Both field selection and analysis were performed in a blinded way.

Proteomic analysis by liquid chromatography coupled to mass spectrometry (LC-MS)

Protein preparation. Cell lysates from $80 \cdot 10^6$ HEK293 cells transfected with 0,6 µg/cm^2 of pcDNA3-myc (control) or pcDNA3-myc-mKV1.3 vectors were collected in RIPA buffer with 1x protease inhibitor (Roche) and after a centrifugation at 10000 g for 10 min at 4ºC the supernatants were incubated with 30 µl of Red Anti-c-Myc Afinity Gel (Sigma). Immunoprecipitates were washed with RIPA buffer with high NaCl (750 mM), Ripa buffer without detergents and finally with 50 mM ammonium bicarbonate.

Mass spectrometry analysis. Proteins were run on a SDS-PAGE gel (10% acrylamide) at 50V. Staining was done using GelCode® Blue Stain Reagent (Thermo Scientific). Gel pieces were cut into cubes (1 mm). For the protein digestion, modified porcine trypsin (Promega) was added at a final ratio of 1:20 (trypsin-protein). Digestion proceeded overnight at 37ºC in 100 mM ammonium bicarbonate, pH 7.8, and the peptide mixtures were subjected to nano-liquid chromatography coupled to mass spectrometry (LC-MS) for protein identification, as previously described (Fernandez-Garcia et al., 2010).

Database searching. Tandem mass spectra were extracted by Proteome Discoverer version 4.1.0.288. All MS/MS samples were analyzed using X! Tandem (The GPM, thegpm.org; version 2007.01.01.1). Mascot and Sequest were up to search MSIPI_mouse_3.67.fasta (56687 entries) assuming the digestion enzyme trypsin. Searches were performed with a fragment ion mass tolerance of 0.90 Da and a parent ion tolerance of 15 PPM. Deamidations, oxidations, acetylations and phosphorylations were specified as variable modifications.

Criteria for protein identification. Scaffold (version Scaffold_4.6.1, Proteome Software Inc., Portland, OR) was used to validate MS/MS based peptide and protein identifications. Peptide identifications were accepted if they could be established at greater than 95.0% probability by the Peptide Prophet algorithm (Keller, Nesvizhskii, Kolker, & Aebersold, 2002). Protein identifications were accepted if they could be

established at greater than 99.9% probability and contained at least 3 identified peptides. Protein probabilities were assigned by the Protein Prophet algorithm (Nesvizhskii, Keller, Kolker, & Aebersold, 2003). Proteins that contained similar peptides and could not be differentiated based on MS/MS analysis alone were grouped to satisfy the principles of parsimony.

Immunoprecipitation

For immunoprecipitation experiments $40x10^6$ HEK293 cells were transfected with 0.06 $\mu g/cm^2$ of Cherry (as control) or Kv1.3-Cherry vectors and incubated in media containing 5 or 20 mM K^+ media, with the Ser/Thr phosphatase inhibitors: NaF (1mM) and okadaic acid (10 mM) for 10-15 min and treated with 250 µM pervanadate (Try phosphatase inhibitor) during the last 5 min of incubation. Cell lysates collected RIPA buffer (150 mM NaCl, 50 mM Tris (pH 8), 1% Nonidet P-40, 0.2% sodium deoxycholate) with 1x protease inhibitor mixture (Halt™, ThermoFisher) were incubated with RFP-Trap_A beads (ChromoTek) for 2–3 h and used for immunoblotting. They were separated by SDS-PAGE in 8% polyacrylamide gels and transferred to nitrocellulose membranes. Mouse monoclonal anti-IQGAP3 antibody (D-10, Santa Cruz Biotechnolgy) was used at a final concentration of 2µg/ml and incubated overnight at 4 °C. Secondary antibody HRP-goat anti-mouse (Dako) was used at final concentration 1:10,000 for 1 h and developed with VersaDoc 4000 Image System (Bio-Rad) using chemiluminescence reagents (SuperSignal West Femto Chemiluminescent Substrate, Pierce).

Imaging of fluorescent-tag proteins

HEK293T cells plated on 12 mm diameter poli-L-lysine coated coverslips were cotransfected with vectors expressing hKv1.3-Cherry (50 ng) and GFP-IQGAP3 (400 ng). After 24 h of incubation cells were fixed with 3.7% paraformaldehyde, nuclei were labelled with Hoechst 33342 (Invitrogen) at 1:4000 and coverslips were mounted in

Vectashield. Photomicrographs were captured with the 63x (1.4 NA) objective of a LEICa SP5 confocal microscope using LAS software.

Immunocytochemistry

Transfected HEK293 cells were plated on round 12 mm diameter poli-L-lysine coated coverslips and kept in culture for 24 h. Afterwards, cells were fixed with 3.7% paraformaldehyde and blocked in PBS with 2% of normal goat serum using a non-permeabilizing blocking solution (without detergents). Cells were incubated at least 2h at RT with rabbit anti-Kv1.3 extracellular primary antibody (APC101, Alomone Labs) at a final concentration of 16 µg/ml, followed by 1 hour incubation with goat anti-rabbit 594 (A-11005, Molecular Probes, 1:1000). After labeling nuclei (Hoechst 33342, 1:4000), coverslips were mounted with Vectashield (Vector Laboratories). Photomicrographs were acquired with a LEICA SP5 confocal microscope using LAS software.

FRET assays

Fluorescence resonance energy transfer (FRET) was used to measure the molecular proximity between Kv1.3 and IQGAP3 by the acceptor photobleaching method measured in discrete ROIs (Albertazzi, Arosio, Marchetti, Ricci, & Beltram, 2009). HEK cells were transiently cotransfected with Kv1.3-Cherry and Kv1.3-GFP (as positive control) or with GFP-IQGAP3. GFP (488ex/494-536em) was used as the donor fluorochrome paired with Cherry (587ex/600-640em) as the acceptor fluorochrome. To measure FRET, four images of donor and acceptor were acquired before and after the photobleaching. The Cherry protein was bleached using maximum laser power. We obtained ~80-90 % of acceptor intensity bleaching. The FRET efficiency was calculated using the equation $[(F_{GFP\_after}-F_{GFP\_before})/F_{GFP\_after}]]$, where F_{GFP_after} and F_{GFP_before} were fluorescence of the donor after and before the bleaching respectively. All images were acquired with a LEICA SP5 confocal microscope using the FRET AB

Wizard in the LAS software. All the experiments were performed with a 63× oil-immersion objective (1.4/NA). All offline image analysis was performed using Image J.

PLA assays

Protein association in transfected HEK cells was explored with PLA technology using the Duolink® In Situ kit (Sigma-Aldrich) and following manufacturer´s instructions. Briefly, HEK cells transfected with Kv1.3-GFP and myc-IQGAP3 were plated in 12 mm diameter dishes and fixed with 4 % paraformaldehyde in PBS. After washings, cells were permeabilized with 0.2% Triton x-100 in PBS and blocked with the kit´s blocking solution at 37 °C for 1 h. Then, cells were incubated with two primary antibodies: 10 µg/ml of Rabbit anti-GFP (Chromtek, PABG1) and 13 µg/ml of mouse anti-myc (Santa Cruz Technologies, sc-40) at room temperature overnight. Cells were then labelled with Duolink® In Situ PLA probes: anti-rabbit MINUS and anti-mouse PLUS for 1 h at 37 °C, followed by ligation and amplification reactions. Samples were mounted with Duolink® In Situ Mounting Media with DAPI to stain the nuclei. Images were acquired with the same settings (gain, filters…) with the 63x oil-immersion objective (1.4/NA) of a LEICA SP5 confocal microscope (Leica Microsystems, Wetzlar, Germany) using LAS software. The PLA signal was recognized as discrete fluorescent spots and was quantified as dots per cell. The negative control samples were incubated only with one primary antibody.

Statistical Analysis

Statistical analysis was performed using Microsoft Excel and R software packages. Pooled data from several different experiments are expressed as mean values ± standard error of the mean (SEM). Shapiro-Wilk test and Bartlett's test were used to test normality and homogeneity of variances respectively. For pairwise comparison of normal distributions, Student's t test was used, otherwise Mann-Whitney U test was applied. For comparisons among several groups, one-way ANOVA followed by Tukey's test was employed in the case of normal distributions and equal variances, alternatively

Kruskal-Wallis analysis followed by Dunn's test was applied. In all cases, differences were considered statistically significant when $p< 0.05$.

RESULTS

Changes in membrane potential affect Kv1.3-induced proliferation

In order to explore if the pro-proliferative role of Kv1.3 in HEK cells is dependent on the voltage-induced conformational changes of the channels, we explored the effects on proliferation of manipulating HEK E_M by co-expressing Kv1.3 channels with the inward-rectifier ATP-dependent K^+ channels (K_{ATP}). We transfected Kir6.2 and SUR1 subunits (the molecular constituents of the cardiac K_{ATP} channels, Flagg et al., 2008), using either the wild type construct (K_{ATP}WT) or a Kir6.2 gain of function mutant (G334D, K_{ATP}GOF). This mutation renders the channel insensitive to cytoplasmic ATP, remaining constitutively open (Masia et al., 2007). Figure 1 shows the effect on proliferation and on E_M of the transfection of HEK cells with each individual channel (Figure 1A) and the cotransfection of Kv1.3 (Figure 1B) or the non-conducting Kv1.3 mutant WF (Cidad et al., 2012; Figure 1C) with K_{ATP}WT or K_{ATP}GOF. Transfection with Kv1.3 channels increased HEK cell proliferation and hyperpolarized E_M from -12.18 ± 2.46 to -41.5 ± 0.75 mV. As expected, transfection of K_{ATP}WT did not change HEK cells E_M while K_{ATP}GOF hyperpolarized the cells to -58.2 ± 2.75 mV, but neither of these two channels modified HEK cell proliferation (Figure 1A). When the coexpression of K_{ATP} and Kv1.3 channels was explored, we found that Kv1.3-induced proliferation was unchanged upon co-transfection with K_{ATP}WT, but was fully abolished in the presence of K_{ATP}GOF (Figure 1B). Similar results were obtained when WF mutant channels were used instead of Kv1.3 (Figure 1C).

K_{ATP}GOF inhibition of Kv1.3-induced proliferation is reverted by depolarization

These results strongly suggest that Kv1.3 or WF induced proliferation is dependent on membrane potential. In order to confirm this, we determined the effect on proliferation of short (15-20 min) incubations of the cells with increased extracellular [K^+] (Figure 2).

As shown in part A of the Figure, proliferation of GFP or K_{ATP}GOF-transfected cells remained at basal levels and was not affected by increasing extracellular [K^+] up to 40 mM. The increased proliferation observed upon transfection with either Kv1.3 or WF was also unchanged when extracellular [K^+] increased. However, the inhibitory effect K_{ATP}GOF on Kv1.3 or WF induced proliferation was progressively reverted by increasing [K^+]. The effect of membrane potential on cell proliferation is more evident when proliferation rate is plotted against the E_M measured in the same cultures with the different $[K^+]_e$ applied (Figure 2B). Whilst proliferation of HEK cells coexpressing Kv1.3 (or WF) and K_{ATP}GOF exhibit a sigmoidal dependence of E_M, it is completely independent of E_M when K_{ATP}GOF are transfected alone. Interestingly, cell depolarization (between -40 and -10 mV) did not modify Kv1.3-induced proliferation when Kv1.3 channels were expressed alone. In order to identify the range of voltages in which Kv1.3 or WF channels undergo voltage-dependent conformational changes, we explored the charge to voltage relationship (Q/V) of the on gating currents (Figure 2C). We found that the Q/V relationship for Kv1.3 channels showed a steeper voltage dependence and is displaced to more negative values when compared to WF. Of interest, in the range of E_M values observed in Kv1.3 transfected cells at the different $[K^+]_e$ applied (the shadowed region in Figures 2B and 2C) the Q_{ON} values for the gating of the channels are already at their maximal value.

Effects on proliferation of Kv1.3 mutants with altered voltage-dependence of activation

The simplest explanation for the previous data is that Kv1.3-induced proliferation relies on voltage-dependent conformational changes of the channels, which in turn activate signaling pathways leading to proliferation. However, we cannot exclude that proliferation inhibition in the presence of K_{ATP}GOF could be due to the high permeability to potassium in this situation, which will effectively clamp membrane potential, inhibiting the changes of E_M needed for cell cycle progression (Levin, 2014; Urrego et al., 2014).

To explore this possibility, we tried an alternative approach. Instead of manipulating E_M, we altered the voltage sensitivity of Kv1.3 channels, by constructing mutant channels whose voltage-dependence of activation were displaced to more depolarized potentials. We benefit from previous published data from Swartz´s laboratory in which they use alanine scanning mutagenesis from S1 to S4 residues of the Kv2.1 channel to examine the mutation-induced perturbation in channel gating (Li-Smerin et al., 2000). We selected three of the described mutations showing a clear rightward shift of the current-voltage curve to test in the Kv1.3 channel (Figure 3A): D285A, (expected $V_{0,5}$=+39.2 mV), A288Y (expected $V_{0,5}$=+66.1mV) and R332A (expected $V_{0,5}$=+104.7mV).

All three mutants expressed functional channels. The current density of the mutants was much lower than the WT Kv1.3 currents, but in all cases was also significantly different from the native K^+ currents recorded in GFP-transfected HEK cells (Figure 3B). In addition, we could detect their expression at the plasma membrane using an extracellular Kv1.3 antibody in non-permeabilized cells (Figure 3C). When looking at the voltage at which currents were first detected, DA and RA mutants showed a rightward shift of 30-40 mV as compared to Kv1.3 currents, while AY mutant did not have any significant difference (Figure 4A, B). As DA and RA currents activate in a range close to endogenous HEK currents, we also explore their sensitivity to Kv1.3 specific blockers to confirm specific expression. Endogenous currents recorded in GFP-transfected cells were insensitive to PAP-1 or Margatoxin (MgTx) application, but all three mutants were inhibited by these blockers in the same range of concentrations that Kv1.3 currents (Figure 4B). The average conductance-voltage curves obtained from WT and mutant channels are shown in Figure 4C.

As expected from the biophysical properties of the currents through these mutant channels, only Kv1.3 or AY transfected cells showed a hyperpolarized E_M in current-clamp experiments. Parallel proliferation studies indicated that only Kv1.3 or AY transfected cells showed a significantly increased proliferation rate, whereas the right-

shifted mutants DA and RA were completely ineffective activating cell proliferation (Figure 4D). Proliferation in RA transfected cells was not stimulated when cells were incubated with 40 mM K^+, suggesting that the depolarization obtained was not sufficient to activate RA channels (data not shown). Moreover, as in the case of the Kv1.3 channels, the effects on proliferation of these gating mutants were also reproduced when the mutations were placed in the pore mutant channel WF (Figure 4E).

Effects on proliferation of voltage-insensitive Kv1.3 mutants.

Our data so far fit the proposed scheme in which Kv1.3 channels behave as voltage-dependent signaling switches. We have previously reported that gating-deficient, voltage-insensitive Kv1.3 channels were not able to induce proliferation, based on the lack of effect of the Kv1.3 mutant channel WF-3X (Cidad et al., 2012). WF-3X channels are non-conducting mutant channels that showed no gating currents, confirming their voltage-insensitivity in the range of potentials explored. As originally described by Miller and Aldrich (Miller & Aldrich, 1996), the apparent lack of voltage-dependent conformational change of this triple mutation in *Shaker* was due to a leftward shift of its activation ($V_{0,5}$ ~ -222 mV). At physiological E_M, these channels should be active, with the pore open and the signaling domain ON. As expected, E_M of cells expressing Kv1.3-3X was very hyperpolarized (almost clamped at E_K, Figure 5A,B), and steady-state inactivation curves showed very little (if any) voltage-dependent inactivation (Figure 5C). Moreover, 200 nM PAP-1 application induced a huge depolarization with a very slow washout in the Kv1.3-3X expressing cells, in contrast with the small and readily reversible effect of PAP-1 on Kv1.3 transfected cells (Figure 5A). However, cells transfected with either Kv1.3-3X channels or with the pore mutant WF-3X (in spite of the large differences in E_M), were unable to reproduce Kv1.3 effects on proliferation (Figure 5D). Furthermore, incubation of Kv1.3-3X- transfected cells with 40 mM extracellular [K^+] depolarized the cells but was not able to induce proliferation.

Kv1.3 associates with IQGAP3

If Kv1.3 is acting as a voltage sensor to induce proliferation, the voltage-dependent transitions must translate into conformational changes of the channel signaling domain leading to the activation of signaling cascades promoting cell proliferation. Previous data obtained both in transfected HEK cells or in native proliferating VSMCs indicated that Kv1.3-dependent proliferation requires the activation of the MEK/ERK signaling pathway and involves channel phosphorylation (Cidad et al., 2015; Jiménez-Pérez et al., 2016), but the identity of these Kv1.3-interacting proteins is not known. Therefore, we searched for potential partners of Kv1.3. Cells transfected with Kv1.3-myc or pcDNA-myc were immunoprecipated with anti-myc. The immunoprecipates were digested with tripsin and the resulting peptides were used for protein identification using LC-MC analysis. From the identified proteins (see supplemental data) associated to Kv1.3 we selected the IQ motif-containing GTPase-activating protein 3 (IQGAP3) as it has been involved in cell proliferation through activation or the MEK/ERK pathway. We have used additional complementary approaches to validate the association between IQGAP3 and Kv1.3 channels. Confocal microscopy images suggest that IQGAP3 colocalize with Kv1.3 in certain areas of the plasma membrane (Figure 6A). Moreover, the association seems to be potentiated by depolarization, since the immunoprecipitation of IQGAP3 with antibodies against the Kv1.3-Cherry channels was only evident when cells were preincubated with high potassium concentrations (Figure 6B). IQGAP3 and Kv1.3 channels colocalize close enough (< 40 nm) to be detected by PLA assays (Figure 7A, B). PLA experiments showed a significant number of fluorescent dots in cells cotransfected with IQGAP3 and Kv1.3. The number of dots was significantly smaller when the association was tested for Kv1.5 channels. Of note, the PLA signal for the IQGAP3-Kv1.3 pair obtained in parallel experiments was larger upon depolarization with 40 mM extracellular [K^+] and smaller in cells cotransfected with K_{ATP}GOF. Same results were obtained when the pair explored was IQGAP3-Kv1.3WF (Figure 7B). However, FRET analysis using IQGAP3-GFP and Kv1.3-Cherry

fusion proteins failed to show a direct association, which could be clearly obtained with a positive control (Kv1.3-Cherry and Kv1.3-GFP fusion proteins, Figure 6E).

Functional role of IQGAP3 in Kv1.3-induced proliferation

In order to explore the possible functional contribution of IQGAP3 to Kv1.3-induced proliferation we studied the effects of overexpressing or silencing IQGAP3 in HEK cells transfected with Kv1.3 channels. Real-time PCR in cells transfected with a combination of 3 different siRNA against IQGAP3 showed a 50% reduction in mRNA levels, that was not observed when transfecting negative control siRNA (Figure 8A). When looking at the proliferation rate in these same cells or in cells co-transfected with Kv1.3 channels, we found that siRNA against IQGAP3 had a small effect on basal HEK cell proliferation and a more pronounced effect in Kv1.3-induced proliferation, demonstrating its participation in the Kv1.3 activated signaling pathway. Of interest, overexpression of IQGAP3 had the same effect than Kv1.3 on HEK cell proliferation, and there was not any additive effect when co-expressing Kv1.3 and IQGAP3, suggesting again that both proteins act through a common signaling pathway (Figure 8C). Finally, the contribution of IQGAP3 to Kv1.3-induced proliferation was also explored in a native system, using primary VSMCs cultures obtained from human arteries (coronary, mammary or renal) or saphenous veins. In all cases, IQGAP3 expression was clearly upregulated in proliferating VSMCs as compared to freshly dissociated, contractile VSMCs (Figure 8D). Moreover, as in the case of HEK cells, siRNA against IQGAP3 was also able to inhibit proliferation in VSMC from human mammary artery (Figure 8E) and saphenous vein (Figure 8F). In this latter preparation, we observed that the inhibitory effect of the Kv1.3 blocker PAP-1 was occluded in the presence of IQGAP3 siRNA, suggesting that also in native systems IQGAP3 may play a role in cell cycle progression through the same signaling pathway that Kv1.3.

DISCUSSION

K^+ channels have been involved in cell proliferation in many systems and tissues, both in physiological and pathological conditions, although a mechanistic understanding of their contribution to cell cycle progression is still missing. Most of the evidences arise from studies showing that cell depolarization or K^+ channel blockade inhibit cell proliferation and often remain just described at a phenomenological level (Wonderlin & Strobl, 1996). Here, using a heterologous expression system and manipulating channel properties with functionally relevant mutations, we have tried to dissect some of the potential mechanisms participating in the crosstalk between Kv1.3 channels and the biochemical pathways linked to proliferation. Kv1.3 channels can modulate cell proliferation by two nonexclusive mechanisms: either regulating E_M (that is, Kv1.3 channels act as E_M modulators) or working as signaling molecules connecting bioelectrical membrane signals with intracellular biochemical pathways (i.e., Kv1.3 channels act as E_M sensors). Although it is likely that in native systems both mechanisms contribute to modulate proliferation (Pérez-García et al., 2018), previous data obtained in HEK cells (Cidad et al., 2012) indicate that the role of Kv1.3 channels as voltage sensors is quite relevant, since they are capable of modulating cell proliferation in the absence of K^+ fluxes. This observation suggest that Kv1.3 do not behave only as K^+ channels, but as integral membrane proteins that can modulate macromolecular complexes (channelosomes) in a voltage dependent manner, mediating key steps in different signal transduction pathways. In this regard, we can hypothesize that in addition to the channel pore, Kv1.3 proteins have a voltage dependent signaling domain (Figure 9) that allows the interaction with signaling molecules. In this work, we have identified IQGAP3 as one of such signaling partners of Kv1.3.

Kv1.3 channels as voltage sensors for cell proliferation

Our current understanding of the correlation between the kinetic properties of Kv currents and the actual conformational changes of the Kv channel proteins is not complete (Barros, Domínguez, & de la Peña, 2012; Kurata & Fedida, 2006; Swartz, 2008). Kinetic behavior of Kv1.3 channels comprise several closed states, a strongly voltage-dependent open state and an inactivated state. Inactivation in Kv1.3 is an example of C-type inactivation, a very complex and poorly understood mechanism of channel closure (Panyi et al., 1995;Kurata and Fedida, 2006). In any case, as the voltage sensor domain determine the conformational changes in the protein that define the conducting properties of the pore (Open/Close transitions), those conformational changes should define the capability of the signaling domain (ON/OFF transitions) to activating proliferative signaling pathways.

Our data indicate that HEK cells proliferation is independent of membrane potential unless they are transfected with Kv1.3 or Kv1.3WF (Figure 2). When Kv1.3 channels are mutated to shift their activation to potentials out of the range of HEK cells E_M (DA and RA, Figures 3 and 4) induction of proliferation does not take place.

In the case of Kv1.3WF, the voltage dependence of proliferation (signaling domain) nicely match the voltage dependence of the gating currents (voltage-sensor domain) whilst in the case of Kv1.3 there are striking differences (Figure 2B and C). Kv1.3 signaling domain seems to be ON at membrane potentials above E_M when high K^+ is used to manipulate E_M and it shows a sigmoidal dependence when cells are cotransfected with K_{ATP}GOF, although the voltage dependence is shifted to depolarized potentials when compared with the voltage dependence of Kv1.3 gating currents. Although this discrepancy is difficult to understand, it has to be noticed that the E_M in Kv1.3 and Kv1.3/K_{ATP}GOF is quite different in normal culturing conditions. When membrane potential was changed with high K^+, E_M was -40 mV when cells were transfected with Kv1.3 and -60 mV when they were cotransfected with K_{ATP}GOF. Moreover, the high permeability to potassium in the later situation could clamp

membrane potential more effectively, inhibiting the putative changes of E_M needed for cell cycle progression.

All these results characterizing the voltage dependence of the proliferative response are compatible with the existence of voltage dependent ON/OFF transitions of the Kv1.3 signaling domain. However, the precise characterization of the voltage dependence of the conformational changes of that domain is not possible with the available technical approaches. We can only take the voltage-dependence of the ionic currents or the gating currents as a readout of the voltage-dependent conformational changes of the whole protein. In that sense, channels can be activated/deactivated (voltage-sensing domain), open/closed (pore domain) and ON/OFF (signaling domain), although the actual voltage dependence of such transitions does not need to be identical.

With respect to the effects of the triple mutants (Kv1.3-3X), and following the previous description of these mutants in *Shaker* (Miller & Aldrich, 1996) we expected to obtain channels fully open in the physiological relevant range of membrane potentials since these channels have a shift of activation to very hyperpolarized potentials. The simplest hypothesis was to assume that these channels should have the signaling domain in an ON state. The Kv1.3-3X currents behave as expected, and channels are open at rest making the membrane potential almost only dependent of the K^+ permeability (Figure 5). However, although Kv1.3-3X channels strongly modulate E_M, they are completely ineffective modulating cell proliferation, as if the signaling domain is in an OFF state. These results suggest that the conformation of these channels in the open state is very different to that of native Kv1.3. The effect of PAP-1 on these mutants supports this hypothesis (Figure 5A). PAP-1 channel blockade involve several sites, being the most relevant the inner-pore and a side-pocket cavity located between the pore and the voltage sensor (Jorgensen et al., 2015). PAP-1 also preferentially binds to residues that become accessible when the channel undergoes C-type inactivation (Schmitz et al., 2005). The PAP-1 effect on Kv1.3-3X channels is larger, with a very slow washout,

strongly suggesting that the conformation of these channels at rest is different from such of native Kv1.3.

Kv1.3 interacting proteins and cell proliferation

The present data support the role of Kv1.3 channels in proliferation as E_M sensors that link changes in membrane potential to proliferative signaling pathways by interacting with signaling molecules. We have tried to shed some light on the Kv1.3-signaling processes by identifying Kv1.3 associated proteins that could participate in the transduction of the voltage-dependent conformational changes of the channel into cytoplasmic or nuclear signals affecting proliferation. Among the several Kv1.3 interacting proteins identified with a proteomic approach (supplemental material), we decided to further characterize IQGAP3. This scaffold protein seemed to be a good candidate for several reasons. IQGAP3 is a member of the IQ motif-containing GTPase-activating proteins, which are scaffolding proteins that facilitate the formation of complexes that regulate growth factor receptor signaling, cytoskeletal dynamics, cell–cell adhesion, migration and proliferation (Monteleon et al., 2015). IQGAP3 is highly expressed in most cancers, and it has been proposed as a novel diagnostic marker and therapeutic target (Monteleon et al., 2015; Xu et al., 2016). Its knockdown inhibits proliferation and its exogenous application induces cell-cycle reentry, indicating that IQGAP3 is necessary and sufficient to drive cell proliferation (Fang et al., 2015; Nojima et al., 2008). IQGAP scaffolds orchestrate EGFR dependent proliferation signaling in cancer cells modulating the MAPK cascade by physically binding to EGFR, MEK1/2, and ERK1/2 (Nojima et al., 2008). This later information is very relevant, as the available data on the signaling pathways involved in Kv1.3-induced proliferation both in native an heterologous systems point to an involvement of MEK/ERK kinases in this effect (Cidad et al., 2012; Jiménez-Pérez et al., 2016). Using several complementary approaches, we could confirm co-localization and association of Kv1.3 and IQGAP3 proteins (Figure 6). As expected, such association seems to be voltage

dependent, since is more probable in high K^+ and less when hyperpolarizing cell with The K_{ATP}GOF mutant (Figure 7). In addition, gain and loss of function experiments demonstrate the functional contribution of IQGAP3 to Kv1.3-induced HEK cell proliferation (Figure 8). In particular, the lack of additive effects on HEK cell proliferation of IQGAP3 and Kv1.3 overexpression suggests that both proteins are modulating proliferation acting through the same signaling pathway. More interesting is the observation that IQGAP3 can have also a relevant role in VSMCs proliferation, as it indicates that at least some of the elements of the signaling pathway described in HEK cells may also contribute to proliferation in the native tissues.

Limitations of the work

The time scale of Kv1.3 voltage dependent transitions affecting ion conduction (ms-s) and proliferation (minutes-hours) are quite different, and the actual value of voltage changes along the cell cycle are not known. We have found some correlation between the steady-state Open/Close and the putative ON/OFF transitions of the channels, but an independent and direct way of measuring conformational changes of the signaling domain is clearly needed.

The voltage range sensed by the voltage sensor domain is best described by the voltage dependence of gating currents, as described for Kv1.3 and Kv1.3WF (Figure 2). However, the lower expression levels of the other mutants precluded the detailed analysis of the gating currents in these constructs (when created in the WF backbone). Although we tried co-expression with Kvβ2 to improve trafficking and increase surface membrane location, we could not get more functional channels with any of these mutants (data not shown).

The absence of FRET between IQGAP3 and Kv1.3 could be related to the location of the fluorophores in the fusion proteins (N-terminal y IQGAP3 and C-Terminal in Kv1.3. We would need to try additional constructs with different location of the fluorophores to confirm these results.

Concluding remarks

The encoding of information by bioelectrical signals requires a high degree of spatial and temporal precision. Molecular dissection of the ion channel proteome and detailed characterization of the functional role of the associated proteins can provide relevant information on how such precision may be achieved. We propose that voltage-dependent conformational changes of the channel protein will determine subtle molecular rearrangements affecting cytoplasmic signaling domains. It is known that the coupling of the voltage sensor movement to operation of the gate involves mainly physical interactions of the S4-S5 linker with the intracellular end of S6 and the cytoplasmic C-linker (Holmgren, Shin, & Yellen, 1998; Lu, Klem, & Ramu, 2002). Either by modulating the gating machinery or by affecting it in response to intracellular modulators, cytoplasmic regions constitute important regulators of voltage-dependent channel gating (Barros et al., 2012). However, details about the conformational rearrangements in the cytoplasmic regions during channel functionality remain mostly unknown. In any case, these voltage-dependent molecular rearrangements could determine the accessibility of several phosphorylation sites in the carboxy terminal domain near the S6 helix, which are essential for Kv1.3-induced proliferation (Jiménez-Pérez et al., 2016). The exposure of these residues upon depolarization (ON state) will allow IQGAP3 interaction, thus initiating the MEK/ERK phosphorylation signaling pathway leading to proliferation.

REFERENCES

Albertazzi, L., Arosio, D., Marchetti, L., Ricci, F., & Beltram, F. (2009). Quantitative FRET analysis with the EGFP-mCherry fluorescent protein pair. *Photochemistry and Photobiology*, *85*(1), 287–297. https://doi.org/10.1111/j.1751-1097.2008.00435.x

Barros, F., Domínguez, P., & de la Peña, P. (2012). Cytoplasmic domains and voltage-dependent potassium channel gating. *Frontiers in Pharmacology*, *3 MAR*(March), 1–15. https://doi.org/10.3389/fphar.2012.00049

Blackiston, D. J., McLaughlin, K. A., & Levin, M. (2009a). Bioelectric controls of cell proliferation: Ion channels, membrane voltage and the cell cycle. *Cell Cycle*, *8*(21), 3527–3536. https://doi.org/10.4161/cc.8.21.9888

Blackiston, D. J., McLaughlin, K. A., & Levin, M. (2009b). Bioelectric controls of cell proliferation: Ion channels, membrane voltage and the cell cycle. *Cell Cycle*. https://doi.org/10.4161/cc.8.21.9888

Cahalan, M. D., & Chandy, K. G. (2009). The functional network of ion channels in T lymphocytes. *Immunol Rev*, *231*(1), 59–87. https://doi.org/10.1111/j.1600-065X.2009.00816.x

Cidad, P., Jiménez-Pérez, L., García-Arribas, D., Miguel-Velado, E., Tajada, S., Ruiz-Mcdavitt, C., … Pérez-García, M. T. (2012). Kv1.3 channels can modulate cell proliferation during phenotypic switch by an ion-flux independent mechanism. *Arteriosclerosis, Thrombosis, and Vascular Biology*, *32*(5), 1299–1307. https://doi.org/10.1161/ATVBAHA.111.242727

Cidad, P., Miguel-Velado, E., Ruiz-McDavitt, C., Alonso, E., Jiménez-Pérez, L., Asuaje, A., … López-López, J. R. (2015). Kv1.3 channels modulate human vascular smooth muscle cells proliferation independently of mTOR signaling pathway. *Pflugers Archiv European Journal of Physiology*, *467*(8), 1711–1722. https://doi.org/10.1007/s00424-014-1607-y

Cidad, P., Moreno-Domínguez, A., Novensá, L., Roqué, M., Barquín, L., Heras, M., … López-López, J. R. (2010). Characterization of ion channels involved in the proliferative response of femoral artery smooth muscle cells. *Arteriosclerosis, Thrombosis, and Vascular Biology*, *30*(6), 1203–1211. https://doi.org/10.1161/ATVBAHA.110.205187

Cone, Jr., C. D. (1970). Variation of the Transmembrane Potential Level as a Basic Mechanism of Mitosis Control. *Oncology*, *24*(6), 438–470. https://doi.org/10.1159/000224545

Cone, C. D. C. M., & Cone, C. D. C. M. (1976). Induction of mitosis in mature neurons in central nervous system by sustained depolarization. *Science*, *192*(4235), 155–158. https://doi.org/10.1126/science.56781

DeCoursey, T. E., Chandy, K. G., Gupta, S., & Cahalan, M. D. (1984). Voltage-gated K+ channels in human T lymphocytes: a role in mitogenesis? *Nature*, *307*(5950), 465–468. https://doi.org/10.1038/307465a0

Fang, X., Zhang, B., Thisse, B., Bloom, G. S., & Thisse, C. (2015). IQGAP3 is essential for cell proliferation and motility during zebrafish embryonic development. *Cytoskeleton*, *72*(8), 422–433. https://doi.org/10.1002/cm.21237

Faouzi, M., Starkus, J., & Penner, R. (2015). State-dependent blocking mechanism of K_v 1.3 channels by the antimycobacterial drug clofazimine. *British Journal of Pharmacology*, *172*(21), 5161–5173. https://doi.org/10.1111/bph.13283

Fernandez-Garcia, B., Casado, P., Prado, M. A., Ugarte-Gil, L. J., Artime, N., Cabal-Hierro, L., … Lazo, P. S. (2010). Proteomic analysis of annexin A2 phosphorylation induced by microtubule interfering agents and kinesin spindle protein inhibitors. *Journal of Proteome Research*, *9*(9), 4649–4660. https://doi.org/10.1021/pr100377v

Feske, S., Wulff, H., & Skolnik, E. Y. (2015). Ion channels in innate and adaptive immunity. *Annual Review of Immunology*, *33*, 291–353. https://doi.org/10.1146/annurev-immunol-032414-112212

Flagg, T. P., Kurata, H. T., Masia, R., Caputa, G., Magnuson, M. A., Lefer, D. J., … Nichols, C. G. (2008). Differential Structure of Atrial and Ventricular K_{ATP}. *Circulation Research*, *103*(12), 1458–1465. https://doi.org/10.1161/CIRCRESAHA.108.178186

Hedman, A. C., Smith, J. M., & Sacks, D. B. (2015). The biology of IQGAP proteins: beyond the cytoskeleton. *EMBO Reports*, *16*(4), 427–446. https://doi.org/10.15252/embr.201439834

Hegle, A. P., Marble, D. D., & Wilson, G. F. (2006). A voltage-driven switch for ion-independent signaling by ether-à-go-go K+ channels. *Proceedings of the National Academy of Sciences of the United States of America*, *103*(8), 2886–2891. https://doi.org/10.1073/pnas.0505909103

Holmgren, M., Shin, K. S., & Yellen, G. (1998). The Activation Gate of a Voltage-Gated K+

Channel Can Be Trapped in the Open State by an Intersubunit Metal Bridge. *Neuron*, *21*(3), 617–621. https://doi.org/10.1016/S0896-6273(00)80571-1

Jiménez-Pérez, L., Cidad, P., Álvarez-Miguel, I., Santos-Hipólito, A., Torres-Merino, R., Alonso, E., … Pérez-García, T. (2016). Molecular determinants of Kv1.3 potassium channels-induced proliferation. *Journal of Biological Chemistry*, *291*(7). https://doi.org/10.1074/jbc.M115.678995

Jorgensen, C., Darré, L., Vanommeslaeghe, K., Omoto, K., Pryde, D., & Domene, C. (2015). In Silico Identification of PAP-1 Binding Sites in the Kv1.2 Potassium Channel. *Molecular Pharmaceutics*, *12*(4), 1299–1307. https://doi.org/10.1021/acs.molpharmaceut.5b00023

Kaczmarek, L. K. (2006). Non-conducting functions of voltage-gated ion channels. *Nature Reviews Neuroscience*, *7*(10), 761–771. https://doi.org/10.1038/nrn1988

Keller, A., Nesvizhskii, A. I., Kolker, E., & Aebersold, R. (2002). Empirical statistical model to estimate the accuracy of peptide identifications made by MS/MS and database search. *Analytical Chemistry*, *74*(20), 5383–5392. https://doi.org/10.1021/ac025747h

Kurata, H. T., & Fedida, D. (2006). A structural interpretation of voltage-gated potassium channel inactivation. *Progress in Biophysics and Molecular Biology*, *92*(2), 185–208. https://doi.org/10.1016/J.PBIOMOLBIO.2005.10.001

Lang, F., Föller, M., Lang, K., Lang, P., Ritter, M., Vereninov, A., … Gulbins, E. (2007). Cell Volume Regulatory Ion Channels in Cell Proliferation and Cell Death. *Methods in Enzymology*, *428*(07), 209–225. https://doi.org/10.1016/S0076-6879(07)28011-5

Levin, M. (2014). Molecular bioelectricity: how endogenous voltage potentials control cell behavior and instruct pattern regulation in vivo. *Molecular Biology of the Cell*, *25*(24), 3835–3850. https://doi.org/10.1091/mbc.e13-12-0708

Li-Smerin, Y., Hackos, D. H., & Swartz, K. J. (2000). alpha-helical structural elements within the voltage-sensing domains of a K(+) channel. *The Journal of General Physiology*, *115*(1), 33–50. https://doi.org/10.1085/jgp.115.1.33

Lu, Z., Klem, A. M., & Ramu, Y. (2002). Coupling between Voltage Sensors and Activation Gate in Voltage-gated K $^{+}$ Channels. *The Journal of General Physiology*, *120*(5), 663–676. https://doi.org/10.1085/jgp.20028696

Masia, R., Koster, J. C., Tumini, S., Chiarelli, F., Colombo, C., Nichols, C. G., & Barbetti, F. (2007). An ATP-Binding Mutation (G334D) in KCNJ11 Is Associated With a Sulfonylurea-Insensitive Form of Developmental Delay, Epilepsy, and Neonatal Diabetes. *Diabetes*, *56*(2), 328–336. https://doi.org/10.2337/db06-1275

McCaig, C. D., Song, B., & Rajnicek, A. M. (2009). Electrical dimensions in cell science. *Journal of Cell Science*, *122*(Pt 23), 4267–4276. https://doi.org/10.1242/jcs.023564

Miguel-Velado, E., Moreno-Domínguez, A., Colinas, O., Cidad, P., Heras, M., Pérez-García, M. T., & López-López, J. R. (2005). Contribution of Kv channels to phenotypic remodeling of human uterine artery smooth muscle cells. *Circulation Research*, *97*(12), 1280–1287. https://doi.org/10.1161/01.RES.0000194322.91255.13

Miller, A. ., & Aldrich, R. . (1996). Conversion of a Delayed Rectifier K+ Channel to a Voltage-Gated Inward Rectifier K+ Channel by Three Amino Acid Substitutions. *Neuron*, *16*(4), 853–858. https://doi.org/10.1016/S0896-6273(00)80105-1

Millership, J. E., Devor, D. C., Hamilton, K. L., Balut, C. M., Bruce, J. I. E., & Fearon, I. M. (2011). Calcium-activated K+ channels increase cell proliferation independent of K+ conductance. *AJP: Cell Physiology*, *300*(4), C792–C802. https://doi.org/10.1152/ajpcell.00274.2010

Monteleon, C. L., McNeal, A., Duperret, E. K., Oh, S. J., Schapira, E., & Ridky, T. W. (2015). IQGAP1 and IQGAP3 Serve Individually Essential Roles in Normal Epidermal Homeostasis and Tumor Progression. *The Journal of Investigative Dermatology*, *135*(9), 2258–2265. https://doi.org/10.1038/jid.2015.140

Nesvizhskii, A. I., Keller, A., Kolker, E., & Aebersold, R. (2003). A statistical model for identifying proteins by tandem mass spectrometry. *Analytical Chemistry*, *75*(17), 4646–4658. https://doi.org/10.1021/ac0341261

Nojima, H., Adachi, M., Matsui, T., Okawa, K., Tsukita, S., & Tsukita, S. (2008). IQGAP3 regulates cell proliferation through the Ras/ERK signalling cascade. *Nature Cell Biology*, *10*(8), 971–978. https://doi.org/10.1038/ncb1757

Ouadid-Ahidouch, H., & Ahidouch, A. (2013). K+ channels and cell cycle progression in tumor cells. *Frontiers in Physiology*, *4 AUG*(August), 1–8. https://doi.org/10.3389/fphys.2013.00220

Panyi, G., Sheng, Z., & Deutsch, C. (1995). C-type inactivation of a voltage-gated K+ channel

occurs by a cooperative mechanism. *Biophysical Journal*, *69*(3), 896–903. https://doi.org/10.1016/S0006-3495(95)79963-5

Pérez-García, M. T., Cidad, P., & López-López, J. R. (2018). The secret life of ion channels: Kv1.3 potassium channels and proliferation. *American Journal of Physiology - Cell Physiology*, *314*(1). https://doi.org/10.1152/ajpcell.00136.2017

Schmitz, A., Sankaranarayanan, A., Azam, P., Schmidt-Lassen, K., Homerick, D., Hansel, W., & Wulff, H. (2005). Design of PAP-1, a selective small molecule Kv1.3 blocker, for the suppression of effector memory T cells in autoimmune diseases. *Molecular Pharmacology*, *68*(5), 1254–1270. https://doi.org/10.1124/mol.105.015669

Smith, J. M., Hedman, A. C., & Sacks, D. B. (2015). IQGAPs choreograph cellular signaling from the membrane to the nucleus. *Trends in Cell Biology*, *25*(3), 171–184. https://doi.org/10.1016/j.tcb.2014.12.005

Sundelacruz, S., Levin, M., & Kaplan, D. L. (2009). Role of membrane potential in the regulation of cell proliferation and differentiation. *Stem Cell Reviews and Reports*, *5*(3), 231–246. https://doi.org/10.1007/s12015-009-9080-2

Swartz, K. J. (2008). Sensing voltage across lipid membranes. *Nature*, *456*(7224), 891–897. https://doi.org/10.1038/nature07620

Tajada, S., Cidad, P., Colinas, O., Santana, L. F., López-López, J. R., & Pérez-García, M. T. (2013). Down-regulation of CaV1.2 channels during hypertension: how fewer CaV1.2 channels allow more Ca2+ into hypertensive arterial smooth muscle. *The Journal of Physiology*, *591*(Pt 24), 6175–6191. https://doi.org/10.1113/jphysiol.2013.265751

Urrego, D., Sánchez, A., Tomczak, A. P., & Pardo, L. A. (2017). The electric fence to cell-cycle progression: Do local changes in membrane potential facilitate disassembly of the primary cilium? *BioEssays*, *1600190*, 1600190. https://doi.org/10.1002/bies.201600190

Urrego, D., Tomczak, A. P., Zahed, F., Stühmer, W., & Pardo, L. A. (2014). Potassium channels in cell cycle and cell proliferation. *Philosophical Transactions of the Royal Society of London. Series B, Biological Sciences*, *369*(1638), 20130094. https://doi.org/10.1098/rstb.2013.0094

Wonderlin, W. F., & Strobl, J. S. (1996). Potassium Channels, Proliferation and G1 Progression. *The Journal of Membrane Biology*, *154*(2), 91–107. https://doi.org/10.1007/s002329900135

Wulff, H., Castle, N. A., & Pardo, L. A. (2009). Voltage-gated potassium channels as therapeutic targets. *Nature Reviews Drug Discovery*, *8*(12), 982–1001. https://doi.org/10.1038/nrd2983

Xu, W., Xu, B., Yao, Y., Yu, X., Cao, H., Zhang, J., … Sheng, H. (2016). Overexpression and biological function of IQGAP3 in human pancreatic cancer. *American Journal of Translational Research*, *8*(12), 5421–5432.

FIGURE LEGENDS

Figure 1. Effect of membrane potential on Kv1.3-induced proliferation.

A-C The right bar graphs show the proliferation rate of control cells (GFP-transfected) or cells transfected with the indicated channels. In all cases, proliferation was determined by measuring the fraction of cells incorporating EdU reagent during a 20 min period. Each bar is the mean ± SEM, n=12–24 determinations from at least five different experiments. The left bar graphs show resting membrane potential (E_M) determinations obtained from cells of the same cultures in current–clamp experiments. Each bar is the mean ± SEM of 10-30 cells from at least four independent experiments. ***p <0.001, compared to GFP transfected cells, ###p < 0.001 compared to Kv1.3 (Figure 1A and B) or to Kv1.3WF (Figure 1C) transfected cells

Figure 2. Effect of membrane potential depolarization on Kv1.3 channel- induced proliferation.

A. The proliferation rate in control conditions or after a short (20 min) incubation at the indicated K^+_e concentrations was measured in cells transfected with GFP (green squares), Kv1.3 alone (black circles) or combined with K_{ATP}GOF (black squares), Kv1.3WF alone (red circles) or combined with K_{ATP}GOF (red squares) and K_{ATP}GOF alone (blue squares). The different K^+_e solutions were applied during the EdU incubation step. The proliferation rate of GFP-transfected cells in basal conditions (5 mM K^+_e) was used for normalization. Each point is the mean ± SEM, n= 6-15 data from at least three independent transfections. **B**. The proliferation rate of the same groups of cells than in A is plotted against the E_M values determined with current clamp experiments in individual cells upon exposure to extracellular solutions with the indicated K^+_e concentrations. Each point is the mean ± SEM, of the normalized proliferation (n= 6-15 data, as in A) against the mean ± SEM of the Em values (n=8-20 determinations in cells from at least two different cultures. C. The plot shows the normalized Q_{ON} voltage dependence of Kv1.3 (black circles) or Kv1.3WF (red circles)

obtained in the absence of permeant ions, using NMDG solutions. Data are mean ± SEM of 4 to 7 different cells in each group. Solid lines represent the data fit to a Boltzmann function. The shadowed area represents the same voltage-range (from -40 to -10 mV) in Figure 2B and 2C.

Figure 3. Construction and expression of Kv1.3 gating mutants.

A. Schematic representation of the different Kv1.3 mutations explored in this work. In addition to the pore mutant Kv1.3-W389F (in red), we have created three point mutations whose equivalents in Shaker channels have been described to produce a rightward shift of the voltage-dependence of activation (in blue). Two of these mutants are in the S3 transmembrane domain (Kv1.3-D285A and Kv1.3-A288Y) and one in the S4 (Kv1.3-R332A). The cartoon also identifies one "voltage-insensitive" Kv1.3 channel (Kv1.3-3X, in green) generated by a triple mutation (R320N/L321A/R326I) in the S4 region, that was previously described to displace the activation $V_{0.5}$ of Shaker channels to potentials bellow -170 mV. Except for this last construct, all the other mutations were also introduced in the Kv1.3-W389F, to create the non-conducting version of the channels. **B.** The plot shows the current density obtained in whole-cell experiments, in cell transfected as indicated with the Kv1.3 gating mutants Kv1.3DA, Kv1.3AY and Kv1.3RA. HEK cells transfected with GFP or with the Kv1.3 WT channels were used as controls. In all cases, the values of current density were obtained from the peak current amplitude recorded in pulses to +80mV from a holding potential of -80 mV. Each bar is the mean ± SEM of 9-16 individual cells from at least 4 different transfections (*p <0.05, **p <0.01; ***p <0.001 with respect to GFP-transfected cells). **C.** Confocal images obtained in HEK cells transfected with vectors expressing the Kv1.3 WT channel or the three mutant channels Kv1.3DA, Kv1.3AY and Kv1.3RA, in all cases as GFP fusion proteins. The panels show the GFP fluorescence (green), the labeling of non-permeabilized cells with an extracellular anti-Kv1.3 channel (red), and the merged images in which the nuclear staining with Hoechst (blue) are also shown.

Figure 4. Functional characterization of Kv1.3 gating mutants.

A. Representative voltage ramps obtained in whole cell experiments from HEK cells transfected with GFP or the Kv1.3 mutant channels as indicated. Ramps were elicited from a holding potential of -80 mV, in control conditions and after application of an external solution containing 200 nM PAP-1. The scale is the same in all cases, to evidence the differences in current amplitude and in the voltage at which currents are first detected. **B.** The current obtained in a similar experiment in a cell transfected with Kv1.3 is shown in the left graph. Here, 2nM MgTx was applied to block Kv1.3 currents. Note the difference in the scale with graphs in A. The bars plot shows the fraction of the current obtained at +40mV that was blocked by the application of PAP1 (200nM, grey bars) or MgTx (2 nM, light grey bars) with each of the indicated constructs. Mean ± SEM, n=4-8 individual cells in each group. **C.** The graph shows the average normalized conductance-voltage relationships and Boltzmann fits for activation obtained from Kv1.3 WT channels and the three mutants (see methods for details). Each data point is the average of 7 individual cells in the case of Kv1.3 and 14-20 cells for the other three constructs. **D.** Proliferation rate of HEK cells transfected with the indicated constructs was determined as a percentage of the proliferation observed in control conditions (GFP-transfected HEK cells). Each bar is the mean ± SEM, n=6-15 data from 3-6 different experiments (***p <0.001 compared to GFP-transfected cells). The lower panel shows E_M determinations obtained from individual cells using current–clamp experiments. Cells were obtained from the same transfections used for determining proliferation rate. Each bar is the mean ± SEM of 7-10 cells from at least 4 independent transfections (*p <0.05 compared to Kv1.3 expressing cells). **E.** Proliferation rate was also determined in HEK cells transfected with the non-conducting version of the Kv1.3 channels (WF mutant) or the three gating mutants, as indicated. Mean ± SEM, n=6-10 data from 3-4 different experiments (*** p <0.001 compared to GFP-transfected cells).

Figure 5. Functional characterization of voltage insensitive Kv1.3 mutants.

A. Representative experiment showing continuous E_M recording obtained from a Kv1.3-3X transfected cell (grey trace, right) or a Kv1.3 expressing cell (black trace, left). During the time indicated by the bars, an external solution containing 40 mM K^+ (K^+) or 200nM PAP-1 (PAP) was applied. Note the differences in E_M in both cells. **B.** The scatter plot shows the average (Mean ± SEM) E_M values obtained in Kv1.3 (filled circles) or Kv1.3-3X (open circles) expressing cells in basal conditions (Rest) or during application of the indicated stimuli (40K, 40 mM K^+_e; PAP, PAP-1 200 nM; MgTx, Margatoxin 2nM). Each point is the average of 5-16 determinations form at least 3 independent experiments (*** p>0,001 compared to Kv1.3). The same results are represented in the right bars plot, but in this case expressed as change in E_M value (ΔVm). **C.** Steady-state activation and inactivation curves were obtained with a two-pulse protocol (shown in the inset in a Kv1.3-3x transfected HEK cell). The peak current amplitude in the prepulse (10 s) was used to create the activation curve (black squares), whereas the inactivation curve (open circles) was obtained by plotting the current amplitude in the pulse (200 ms) to +40mV as a function of the voltage of the prepulse. In both cases, normalized currents (using the current amplitude at +40mV) are represented. Each point is mean ± SEM, n=6 cells. **D.** Proliferation rate was determined by measuring the fraction of cells incorporating EdU during a 20 min period. HEK cells were transfected as indicated with GFP, Kv1.3 WT channels or the Kv1.3-3X or Kv1.3WF-3X mutants. Also, the proliferation rate of Kv1.3 and Kv1.3-3X expressing cells after 20 min incubation with 40 mM K^+_e was measured. Each bar represents the mean ± SEM (n=6-9 data from 3 different experiments; ***p <0.001 compared to GFP-transfected cells). The lower plot shows E_M determinations obtained from individual cells from the same transfections (n=8-10 cells; *** p <0.001 compared to Kv1.3 transfected cells

Figure 6. Kv1.3 Associates with IQGAP3.

A. Confocal images of HEK cells cotransfected with GFP-IQGAP3 and Kv1.3-Cherry plasmids. The panels show the fluorescence of IQGAP3 (green), of Kv1.3 (red) and the merged images with the nuclei stained with Hoechst (blue). **B.** Representative immunoblot obtained with anti-IQGAP3 antibody on HEK cells transfected with Cherry (C) or Kv1.3-Cherry incubated 10 minutes with 5 or 20 mM of K^+_e solution. The upper immunoblot shows total cell lysates, the lower immunoblot shows the same lysates after immunoprecitipitation with RFP-Trap.

Figure 7. Kv1.3 association with IQGAP3 is voltage-dependent.

A. Representative confocal images showing the merged fluorescence of dot distribution of PLA signal (red), the GFP-labelling of Kv1.3 channels (green) and the nuclei stained with DAPI (blue). The panels show HEK cells transfected with myc-IQGAP3 in combination with Kv1.3-GFP alone in basal conditions (5 mM K^+_e, upper panel), after 10 min incubation with 40 mM K^+_e, (middle panel) or with Kv1.3-GFP in combination with K_{ATP}GOF (lower panel). **B.** The bar plots represents PLA signal quantification by determining the average dots per cell in cells cotransfected with IQGAP3 and the indicated channels: Kv1.5, Kv1.3 or Kv1.3WF alone or with K_{ATP}GOF. In the case of Kv1.3 PLA signals were also measured with 40 mM K^+_e, The PLA signals were obtained using anti-Myc and anti-GFP antibodies, and negative control were obtained by incubation with only one primary antibody. The average dots in cells transfected with IQGAP3 and Kv1.3 (control) was use for normalization. Mean ± SEM, n=10-25 cells from at least 2 different transfections. *p<0.05; **p<0.01; ***p <0.001, compared to Kv1.3 transfected cells in basal conditions, $^{\#\#}$p<0.001 compared to Kv1.3WF transfected cells. **C.** Bar plot shows FRET efficiency in HEK cells co-transfected with Kv1.3-Cherry and GFP-IQGAP3 in control media or in 20 mM K^+_e. As positive control cells were co-transfected with Kv1.3-GFP and Kv1.3-Cherry. Data are mean ± SEM,

10-25 cells in each group from 4 independent experiments. The inset shows an example of the fluorescence values (in arbitrary units) of the donor (GFP, green line and symbols) and the acceptor (Cherry, red lines and symbols) in a stack of 8 images with acceptor photobleaching between images four and five, of the positive control (filled circles) and the experimental condition (empty squares)

Figure 8. Functional contribution of IQGAP3 to proliferation. A. Determination of IQGAP3 mRNA expression levels in response to transfections with siRNAs against IQGAP3 or a negative control siRNA (Si C-) in HEK cells or VSMCs from human saphenous veins (hSV). Expression data are normalized with the $2^{-\Delta\Delta Ct}$ method, using the mock transfected cells (control) as calibrator (see methods). Mean ± SEM; n=4-6 data from 2-3 different experiments **B.** Proliferation rate of HEK cells transfected with either GFP or Kv1.3-GFP alone as indicated (Control, white columns) or together with the negative control siRNA (si C-, grey columns) or the IQGAP3 siRNA (si IQGAP3, black columns). Each bar is the mean (± SEM) of 8-9 data from 3 different experiments. *** p <0.001 compared to Kv1.3 + si C- transfected cells**. C.** Proliferation rate was measured in control HEK cells (transfected with Cherry) or cells transfected with Kv1.3-Cherry (Kv1.3), IQGAP3-GFP (IQGAP3) or Kv1.3 and IQGAP3 together (Kv1.3+IQGAP3). Mean ± SEM; n=9 data from 3 different experiments. **D.** IQGAP mRNA abundance was determined in VSMCs obtained from human saphenous vein (hSV), mammary artery (hMA), renal artery (hRA) and coronary artery (hCA). In each case, mRNA was measured from VSMCs dispersed from the vessel wall (Tissue, black bars) of VSMC in primary cultures obtained from explants (Culture, white bars). IQGAP3 mRNA was normalized using RPL18 as endogenous control, and expressed as $2^{-\Delta Ct}$. Each bar is the mean of at least 3 independent determinations by triplicate. **E.** Proliferation rate of cultured VSMCs from human mammary artery transfected with the negative control siRNA (si C-) or the IQGAP3 siRNA (si IQGAP·) using PDGF (20ng/µl) as mitogenic stimuli. Data are mean ± SEM, n=14-15 determinations form 5 different

experiments. **p <0.01 compared to si C- transfected cells**. F.** Cultured VSMCs from human saphenous veins were transfected with negative control siRNA (si C-) or , IQGAP3 siRNA (si IQGAP3) as indicated, and proliferation rate in response to 24h treatment with 20 ng/µl or PDGF alone (control, white bars) or in combination with 100 nM PAP-1 (grey bars) was measured. Each bar is the mean ± SEM of 5-7 determinations obtained form 3 independent experiments. * p <0.05 compared to control.

Figure 9. Scheme of the proposed mechanism. Our data indicate a correlation between voltage-dependent conformational changes of Kv1.3 channels and activation of proliferation. We propose that the Kv1.3 signaling domain, located in the C-terminal intracellular region, can fluctuate between ON and OFF states. In the ON state, it can bind other adapter/associated proteins that promote cell cycle progression.

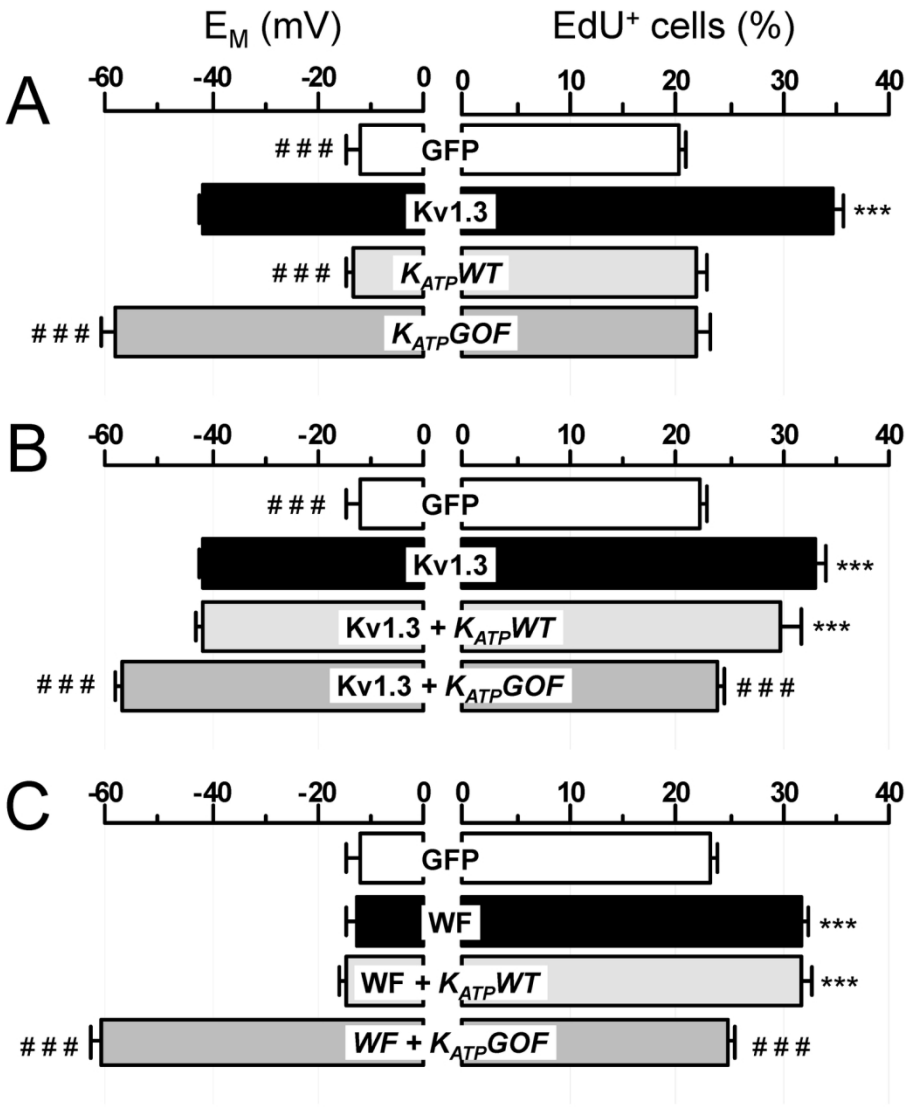

Figure 1

149x175mm (300 x 300 DPI)

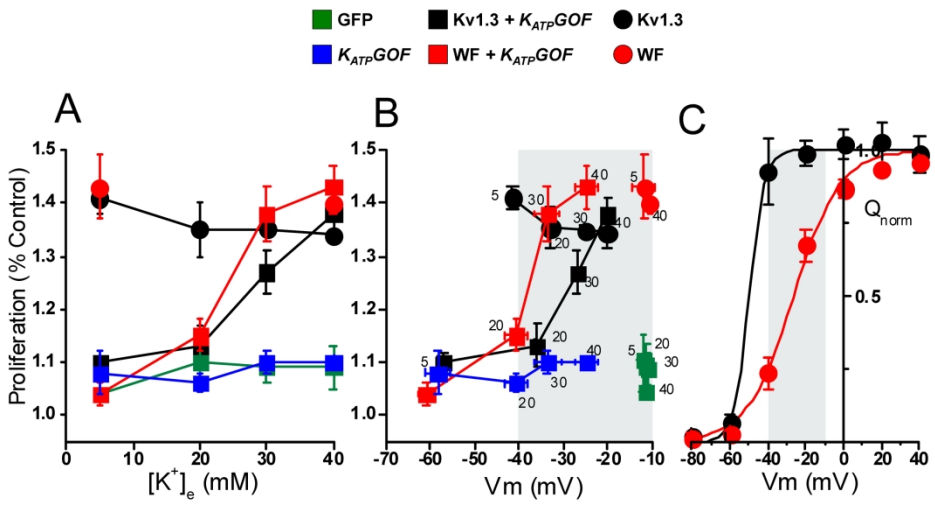

Figure 2

244x137mm (300 x 300 DPI)

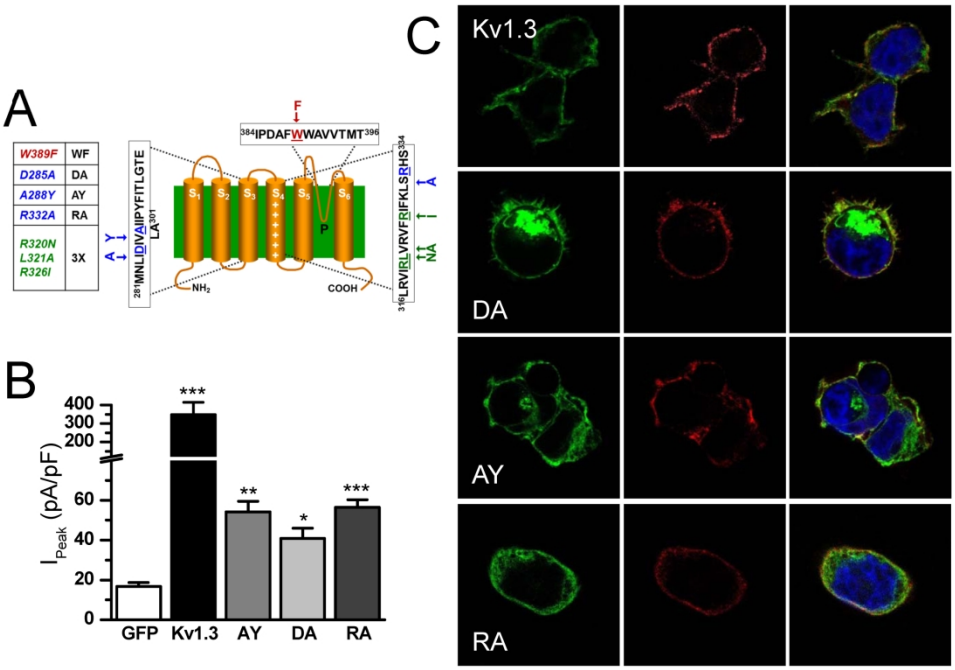

Figure 3

247x169mm (300 x 300 DPI)

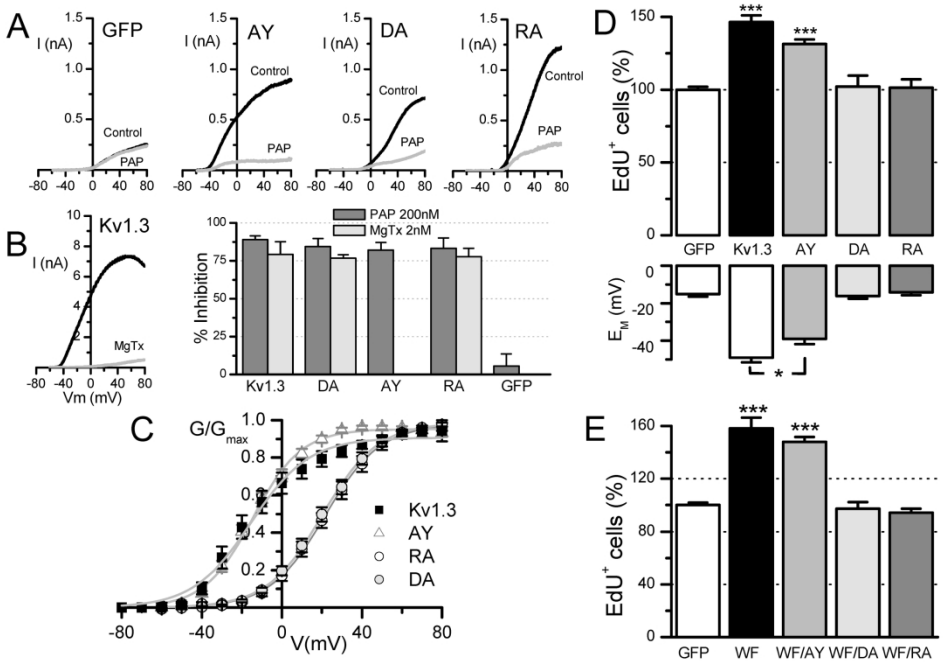

Figure 4

237x167mm (300 x 300 DPI)

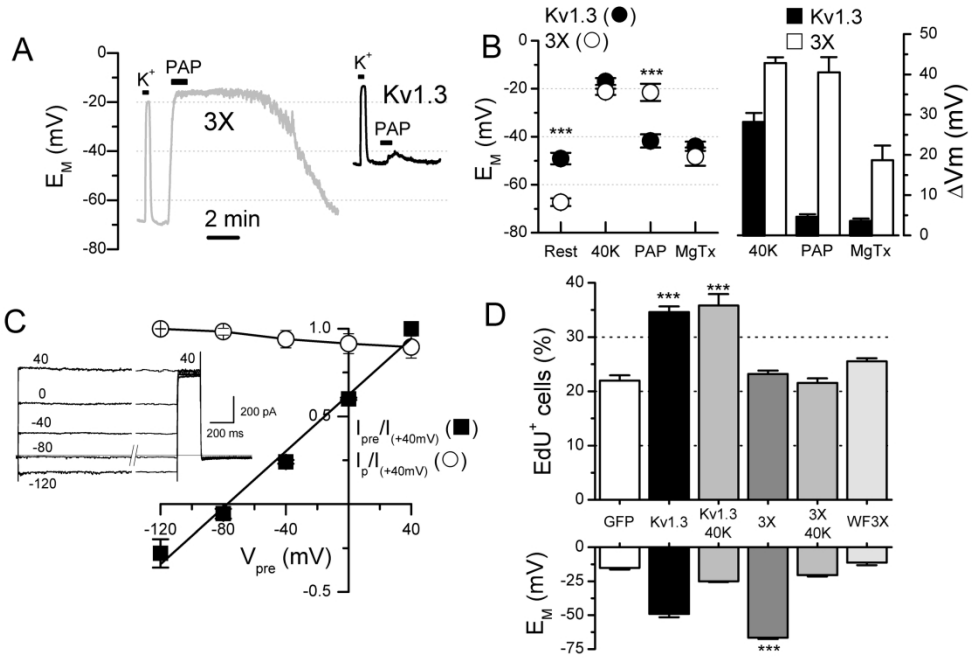

Figure 5

236x164mm (300 x 300 DPI)

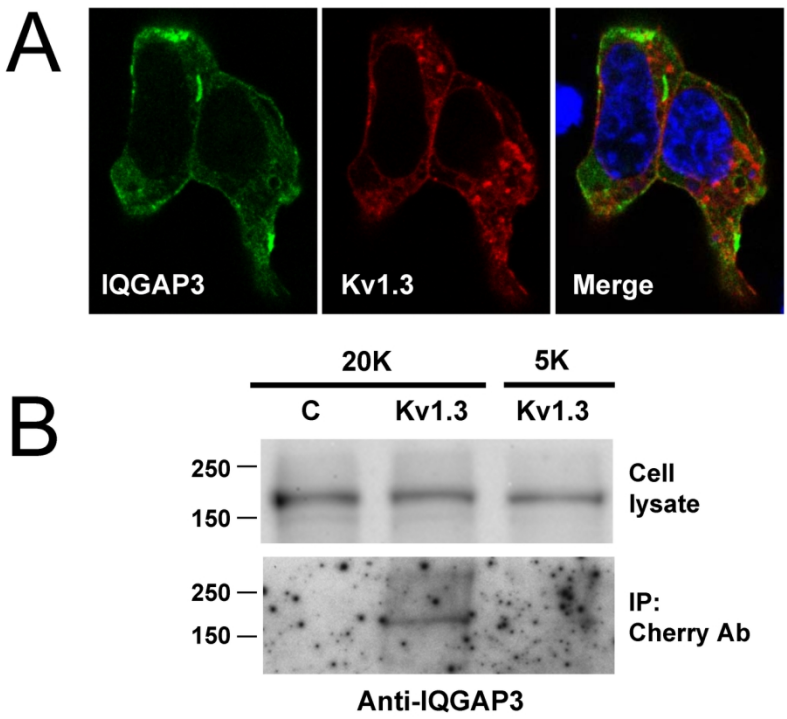

Figure 6

153x132mm (300 x 300 DPI)

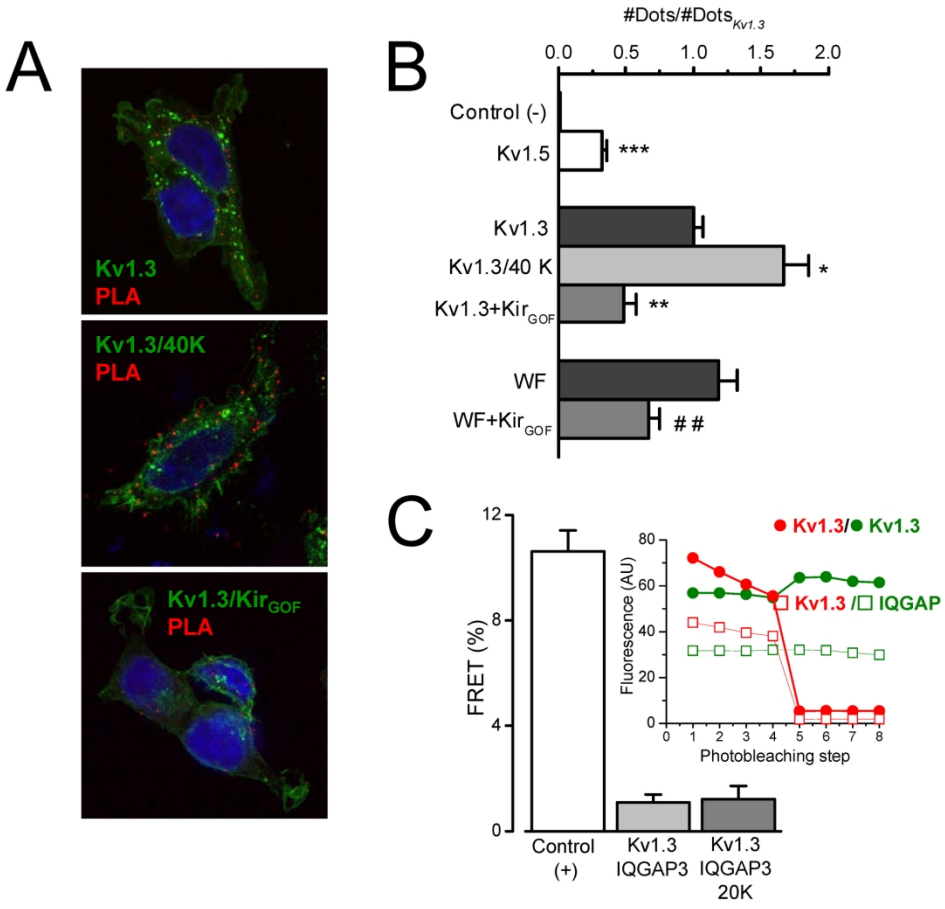

Figure 7

182x170mm (300 x 300 DPI)

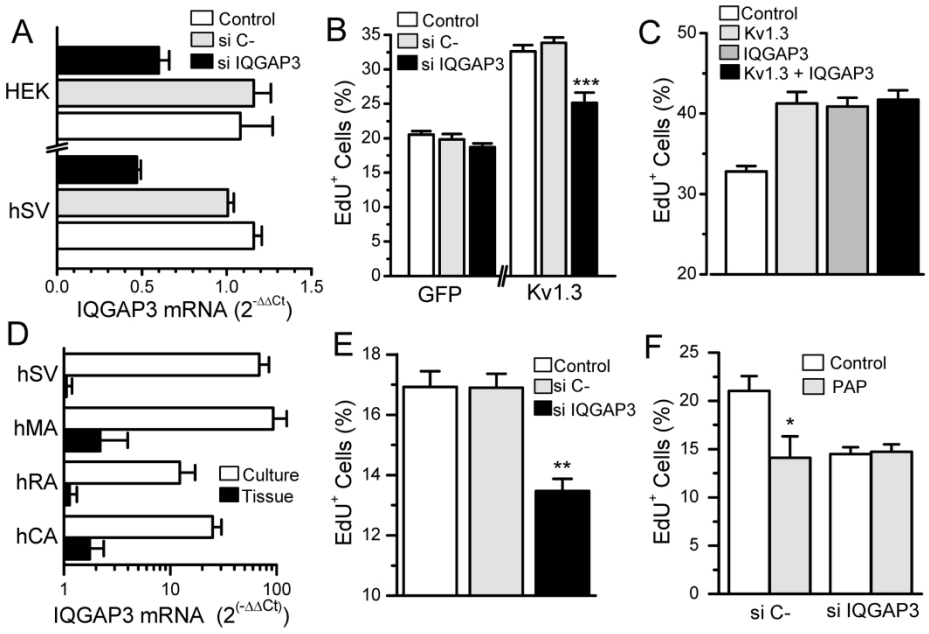

Figure 8

239x166mm (300 x 300 DPI)

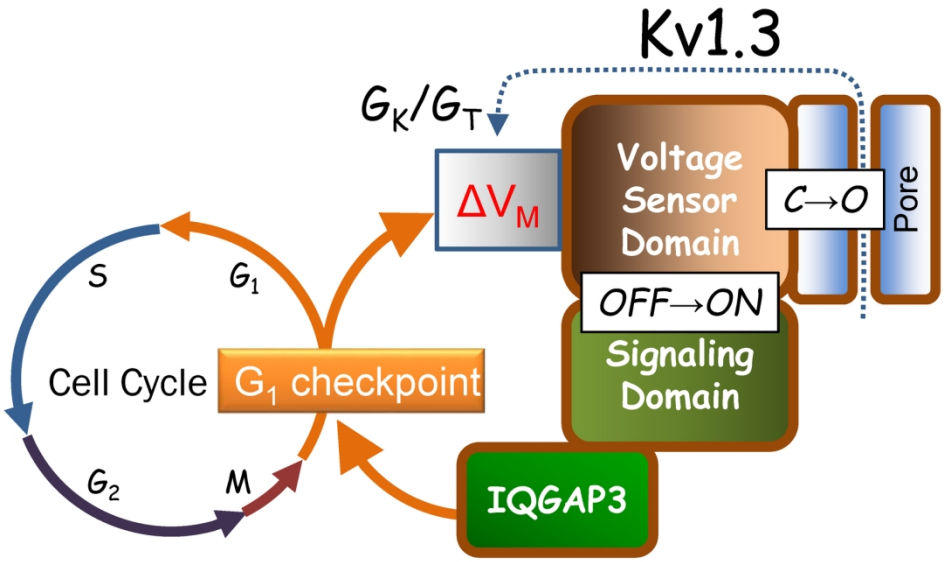

Figure 9

159x100mm (300 x 300 DPI)